arXiv:1601.01125v2 [stat.CO] 1 Dec 2016

The Gibbs Sampler with Particle Efficient Importance Sampling for State-Space Models*

Oliver Grothe
Institute of Operations Research, Karlsruhe Institute of Technology, Germany

Tore Selland Kleppe
Department of Mathematics and Natural Sciences, University of Stavanger, Norway

Roman Liesenfeld†
Institute of Econometrics and Statistics, University of Cologne, Germany

(November 19, 2016)

Abstract

We consider Particle Gibbs (PG) as a tool for Bayesian analysis of non-linear non-Gaussian state-space models. PG is a Monte Carlo (MC) approximation of the standard Gibbs procedure which uses sequential MC (SMC) importance sampling inside the Gibbs procedure to update the latent and potentially high-dimensional state trajectories. We propose to combine PG with a generic and easily implementable SMC approach known as Particle Efficient Importance Sampling (PEIS). By using SMC importance sampling densities which are closely globally adapted to the targeted density of the states, PEIS can substantially improve the mixing and the efficiency of the PG draws from the posterior of the states and the parameters relative to existing PG implementations. The efficiency gains achieved by PEIS are illustrated in PG applications to a univariate stochastic volatility model for asset returns, a Gaussian nonlinear local-level model for interest rates, and a multivariate stochastic volatility model for the realized covariance matrix of asset returns.

JEL classification: C11; C13; C15; C22.

Keywords: Ancestor sampling; Dynamic latent variable models; Efficient importance sampling; Markov chain Monte Carlo; Sequential importance sampling.

*An earlier version of the paper circulated under the title "Bayesian Analysis in Non-linear Non-Gaussian State-Space Models using Particle Gibbs".

†Corresponding address: Institut für Ökonometrie und Statistik, Universität Köln, Universitätsstr. 22a, D-50937 Köln, Germany. Tel.: +49(0)221-470-2813; fax: +49(0)221-470-5074. *E-mail address:* liesenfeld@statistik.uni-koeln.de (R. Liesenfeld)

1. Introduction

State space models (SSM) are a popular class of dynamic models used to analyze time series. In the context of SSMs, a latent Markov state variable x_t $(t = 1, \ldots, T)$ is observed through a response variable y_t, where it is assumed that the y_t's are conditionally independent given the x_t's. The measurement density for y_t and the transition density for x_t, depending on a vector of parameters θ are written as

$$y_t|x_t \sim g_\theta(y_t|x_t) \qquad \text{and} \qquad x_t|x_{t-1} \sim f_\theta(x_t|x_{t-1}), \quad x_1 \sim f_\theta(x_1), \tag{1}$$

respectively. Bayesian inference about the parameters θ and the states $x_{1:T}$ relies on their joint posterior denoted by $p(\theta, x_{1:T}|y_{1:T})$, where we have used the notation $z_{s:t}$ to denote $(z_s, z_{s+1}, \ldots, z_t)$. The corresponding marginal posterior for the parameters is $p(\theta|y_{1:T}) \propto p_\theta(y_{1:T})p(\theta)$, where $p(\theta)$ denotes the prior assigned to θ and $p_\theta(y_{1:T})$ the marginal likelihood. For non-linear, non-Gaussian models, both the joint posterior of θ and $x_{1:T}$ as well as the marginal posterior for θ are analytically intractable so that inference requires to resort to approximation techniques.

A new and easy to implement tool for approximating the joint posterior $p(\theta, x_{1:T}|y_{1:T})$ in SSMs are the Particle Markov Chain Monte Carlo (PMCMC) algorithms developed by Holenstein (2009) and Andrieu et al. (2010), which combine standard Markov Chain Monte Carlo (MCMC) procedures with sequential Monte Carlo (SMC) algorithms. The latter are simulation devices for approximating high-dimensional target densities such as the conditional posterior of the states in SSMs denoted by $p_\theta(x_{1:T}|y_{1:T})$. More specifically, SMC methods generate a swarm of $x_{1:t}$-samples (particles), that evolve towards the target distribution according to a combination of sequentially importance sampling (IS) and resampling. Standard SMC implementations rely upon locally designed IS densities approximating sequentially period by period the corresponding subcomponents of the full target density (see, e.g., Gordon et al., 1993, Pitt and Shephard, 1999, and Doucet and Johansen, 2009). Within the PMCMC approach such SMC algorithms are used in order to design proposal densities for Metropolis-Hastings (MH) updates producing MCMC draws from the respective target density.

A PMCMC algorithm available for a full Bayesian analysis in SSMs is the Particle Gibbs (PG) (Andrieu et al., 2010, and Chopin and Singh, 2013). It represents an MC approximation of an 'ideal' (but infeasible) Gibbs algorithm that updates the joint posterior $p(\theta, x_{1:T}|y_{1:T})$ by alternately sampling from the full conditional posterior of the states $p_\theta(x_{1:T}|y_{1:T})$ and the full conditional posterior of the parameters denoted by $p(\theta|x_{1:T}, y_{1:t})$. Within PG the output of an SMC algorithm targeting $p_\theta(x_{1:T}|y_{1:T})$ is used as a proposal

distribution for MH updates of $x_{1:T}$. While easy to implement, the baseline PG is known to suffer in applications with large T from a poor mixing since the resampling in SMC procedures leads to a path degeneracy of the particle system hampering a sufficiently fast exploration of the domain of $x_{1:T}$ under $p_\theta(x_{1:T}|y_{1:T})$ (Whiteley et al., 2010 and Lindsten and Schön, 2012). Existing attempts to address this structural poor mixing problem of the PG are to either add a Backward Simulation step (PGBS) (Whiteley, 2010, Whiteley et al., 2010, Lindsten and Schön, 2012, and Carter et al., 2014) or an Ancestor Sampling step (PGAS) (Lindsten et al., 2014) to the SMC algorithm, or to introduce an additional MH move to update $x_{1:T}$ (PGMH) (Holenstein, 2009, p. 35). Nevertheless, the efficacy of those extensions to improve the mixing of the baseline PG critically depends on how close the underlying SMC algorithm approximates the target $p_\theta(x_{1:T}|y_{1:T})$.

In this paper we propose to combine PG and its PGAS and PGMH extensions with a conditional version of the Particle Efficient Importance Sampling (PEIS) recently developed by Scharth and Kohn (2016). PEIS is a 'forward-looking' SMC procedure which relies on the Efficient IS (EIS) technique of Richard and Zhang (2007) for designing efficient SMC IS densities. This approach exploits that EIS produces by a sequence of simple auxiliary regressions a close global density approximation to potentially high-dimensional target densities. Scharth and Kohn (2016) uses PEIS to obtain unbiased and highly accurate SMC estimates of the marginal likelihood $p_\theta(y_{1:T})$ for an MH procedure targeting directly the marginal posterior of the parameters $p_\theta(\theta|y_{1:T})$. Here we extend the application of PEIS and show formally how it can be used within PG to construct valid novel high dimensional MCMC kernels to simulate from the joint posterior $p(\theta, x_{1:T}|y_{1:T})$.

Moreover, we complement Scharth and Kohn's (2016) discussion of the PEIS by providing further important insight into the design of the PEIS. In particular, we show that it defines an SMC where in each period t both the sequential IS sampling as well as the resampling are close to be optimally globally adapted to the full targeted posterior $p_\theta(x_{1:T}|y_{1:T})$. Based on this insight we can analytically show that PEIS is capable to substantially improve the mixing of the PGAS and PGMH relative to their implementations using standard locally designed SMC procedures. Striking empirical illustrations of how the PEIS improves this mixing are provided in Sections 5 and 6, where we apply PG algorithms to a Bayesian analysis of a univariate stochastic volatility model (SV) for asset returns, a univariate time-discretized Constant Elasticity of Variance (CEV) diffusion for interest rates, and a multivariate SV model for the realized covariance matrices of a vector of asset returns.

An alternative PMCMC procedure to the PG approach is the particle marginal MH (PMMH) (Holen-

stein, 2009 and Andrieu et al., 2010). It is an MC approximation of the 'ideal' MH procedure targeting directly the marginal posterior density $p(\theta|y_{1:T})$ and marginalizes the states $x_{1:T}$ by using SMC to obtain an unbiased MC estimate of the marginal likelihood $p_\theta(y_{1:T})$. Applications of PMMH for Bayesian inference in SSMs are found in Fernandez-Villaverde and Rubio-Ramirez (2005), Flury and Shephard (2011) and Pitt et al. (2012), where PMMH is implemented with standard locally designed SMC procedures, and in Scharth and Kohn (2016) who use PEIS for PMMH implementations. However, a potential drawback of the PMMH approach is, that the design of a proposal density for the MH updates of θ can be tedious, requiring a fair amount of fine tuning, especially, when the number of parameters in θ are large. Moreover, in multivariate SSMs with high-dimensional state vectors x_t a sufficiently accurate SMC estimation of the marginal likelihood $p_\theta(x_{1:T})$ as required for PMMH can be computationally very difficult (Flury and Shephard, 2011). The advantage of PG procedures, including our proposed PG-PEIS approach, is that they offer in many applications to bypass those problems. In particular, PG can take advantage of the fact that sampling from $p(\theta|x_{1:T}, y_{1:t})$ is often easily feasible so that the tedious design of a proposal for the marginal MH update of θ can be avoided. Also PG does not need to MH update $x_{1:T}$ in one block so that SMC sampling from $p_\theta(x_{1:T}|y_{1:t})$ can be partitioned into a sequence of smaller sampling problems. This can be a partitioning into blocks along the time dimension and/or into state components for high-dimensional state vectors x_t. Those potential advantages of PG in SSMs with many state components and/or parameters are empirically illustrated in our application of the PG-PEIS approach to the multivariate SV model for realized covariance matrices, which involves five latent state processes and 26 parameters.

The rest of the paper is organized as follows: In Section 2 we briefly outline the SMC approach and in Section 3 the baseline PG. Section 4 presents the PEIS as well as the PG-PEIS approach (Section 4.1) and discusses potential efficiency improvements obtained by embedding the PEIS within the PGAS (Section 4.2) and the PGMH (Section 4.3). This is illustrated in Section 5 with a Bayesian PG analysis of a univariate SV model and a CEV model and in Section 6 with a multivariate SV specification. Section 7 concludes.

2. Sequential Monte Carlo (SMC)

2.1 Definition of SMC

Let $\pi(x_{1:T})$ denote the target density to be approximated/simulated with the following sequence of intermediate target densities:

$$\pi_t(x_{1:t}) = \frac{\gamma_t(x_{1:t})}{z_t}, \qquad z_t = \int \gamma_t(x_{1:t}) dx_{1:t}, \qquad t = 1, \ldots, T, \tag{2}$$

with $\pi_T(x_{1:T}) \equiv \pi(x_{1:T})$.

In an SSM of the form given by Equation (1) the full target is $\pi(x_{1:T}) = p_\theta(x_{1:T}|y_{1:T})$ and for standard SMC algorithms the intermediate targets are defined as $\pi_t(x_{1:t}) \equiv p_\theta(x_{1:t}|y_{1:t})$, so that we have

$$\gamma_t(x_{1:t}) = p_\theta(x_{1:t}, y_{1:t}) = \left[\prod_{\tau=2}^{t} g_\theta(y_\tau|x_\tau) f_\theta(x_\tau|x_{\tau-1})\right] g_\theta(y_1|x_1) f_\theta(x_1), \tag{3}$$

$$z_t = p_\theta(y_{1:t}) = \int p_\theta(x_{1:t}, y_{1:t}) dx_{1:t}, \tag{4}$$

where the sequence $z_t = p_\theta(y_{1:t})$ represent the marginal likelihoods.

SMC algorithms as discussed, e.g., in Cappé et al. (2007), Ristic et al. (2004) and Doucet and Johansen (2009), consist of recursively producing, for each period t, a weighted particle system $\{x^i_{1:t}, w^i_t\}_{i=1}^N$ with N particles $x^i_{1:t}$ and corresponding (non-normalized) IS weights w^i_t such that the intermediate target density $\pi_t(x_{1:t})$ in Equation (2) can be approximated by the point mass distribution

$$\hat{\pi}_t(dx_{1:t}) = \sum_{i=1}^{N} W^i_t \, \delta_{x^i_{1:t}}(dx_{1:t}), \qquad W^i_t = \frac{w^i_t}{\sum_{l=1}^N w^l_t}, \tag{5}$$

where $\delta_x(\cdot)$ denotes the Dirac delta mass located at x. In period t, the weighted particle system $\{x^i_{1:t}, w^i_t\}_{i=1}^N$ is obtained from the period-$(t-1)$ system $\{x^i_{1:t-1}, w^i_{t-1}\}_{i=1}^N$ by drawing from an IS-density $q_t(x_t|x^i_{1:t-1})$ to propagate the inherited particles $x^i_{1:t-1}$ to $x^i_{1:t} = (x^i_t, x^i_{1:t-1})$ and updating the corresponding IS weights according to

$$w^i_t = W^i_{t-1} \frac{\gamma_t(x^i_{1:t})}{\gamma_{t-1}(x^i_{1:t-1}) q_t(x^i_t|x^i_{1:t-1})}. \tag{6}$$

In most applications, the variance of the IS weights w^i_t in Equation (6) increases exponentially with t reducing the effective sample size of the particle system (an effect known as 'weight degeneracy'). Hence, SMC algorithms include a resampling step before propagating the particles $x^i_{1:t-1}$ to $(x^i_t, x^i_{1:t-1})$.

It consists in sampling N 'ancestors particles' from $\{x^i_{1:t-1}\}_{i=1}^N$ according to their normalized IS weights $\{W^i_{t-1}\}$ and then setting in Equation (6) the IS weights W^i_{t-1} for the redrawn $x^i_{1:t-1}$-particles all equal to $1/N$. This resampling step amounts to sampling for $t = 2, ..., T$ the (auxiliary) indices of the ancestor particles $x^i_{1:t-1}$ denoted by a^i_t. For a discussion of popular resampling schemes including multinomial, residual and stratified resampling, see, e.g., Doucet and Johansen (2009).

At period T, this procedure provides us with an approximation of the full target density $\pi(x_{1:T})$ given by $\hat{\pi}_T(dx_{1:T})$ according to Equation (5). Approximate samples from $\pi(x_{1:T})$ can be obtained by sampling $x^i_{1:T} \sim \hat{\pi}_T(dx_{1:T})$, which is done by choosing particles $x^i_{1:T}$ according to their probabilities W^i_T. If required, the corresponding normalizing constant z_T of $\pi(x_{1:T})$ is estimated by

$$\hat{z}_T = \prod_{t=1}^{T} \left(\sum_{i=1}^{N} w^i_t \right). \tag{7}$$

In the SSM context, such an SMC produces an approximation of $\pi(x_{1:T}) = p_\theta(x_{1:T}|y_{1:T})$, denoted by $\hat{p}_\theta(x_{1:T}|y_{1:T})$, corresponding approximate samples $x^i_{1:T} \sim \hat{p}_\theta(x_{1:T}|y_{1:T})$, and an MC approximation to the full marginal likelihood $z_T = p_\theta(y_{1:T})$ written as $\hat{p}_\theta(y_{1:T})$. These are the main inputs of PG algorithms implemented for Bayesian analyzes of SSMs.

2.2 SMC implementations in state space models

A critical issue in implementing an SMC is the choice of the IS densities $q_t(x_t|x^i_{1:t})$. The main recommendation is to design them *locally* so as to minimize the conditional variance of the IS weights in Equation (6) given $x^i_{1:t-1}$. This requires to select $q_t(x_t|x^i_{1:t-1})$ as a close approximation to the period-t conditional density $\pi_t(x_t|x^i_{1:t-1})$ (see Doucet and Johansen, 2009). For the SSM applications with $\pi_t(x_{1:t}) \propto p_\theta(x_{1:t}, y_{1:t})$ as given by Equation (3), those IS weights become

$$w^i_t = W^i_{t-1} \frac{g_\theta(y_t|x^i_t) f_\theta(x^i_t|x^i_{t-1})}{q_t(x^i_t|x^i_{1:t-1})}. \tag{8}$$

The most popular (but suboptimal) selection for the IS densities are the transition densities $f_\theta(x_t|x^i_{t-1})$ used by the Bootstrap Particle Filter (BPF) (Gordon et al., 1993). In scenarios where the measurement density g_θ is fairly flat in x_t, this selection typically leads to a satisfactory performance. A selection which sets the variance of the IS weights in Equation (8) *conditional on* x^i_{t-1} to zero is $p_\theta(x_t|y_t, x^i_{t-1}) \propto g_\theta(y_t|x_t) f_\theta(x_t|x^i_{t-1})$, leading to the conditionally Optimal Particle Filter (OPF) discussed, e.g., in Doucet

and Johansen (2009). Further improvements can be achieved by replacing the standard resampling schemes based on the IS weights in Equation (8) by more sophisticated ones which favor ancestor particles which will be in regions with high probability mass after their propagation. This is implemented by the Auxiliary Particle Filter (APF) (Pitt and Shephard, 1999).

In contrast to those locally designed SMCs, the PEIS of Scharth and Kohn (2016) uses (nearly) *globally* optimal SMC-IS densities and resampling weights obtained from a close approximation to the full target $\pi(x_{1:T}) = p_\theta(x_{1:T}|y_{1:T})$. This will be explained in greater detail in Section 4.1 below.

Irrespectively of the particular IS density selected to implement an SMC, the resampling steps used to mitigate the weight degeneracy, typically lead to a loss of diversity among the particles as the resultant sample may contain many repeated points. Hence, in many SMC applications resampling is performed dynamically, i.e., only when the weight degeneracy exceeds a certain threshold (see, e.g., Doucet and Johansen, 2009).

3. Particle Gibbs (PG)

3.1 Baseline Particle Gibbs algorithm

For a Bayesian analysis in a non-linear, non-Gaussian SSM the 'ideal' Gibbs sampler targeting the joint posterior $p(\theta, x_{1:T}|y_{1:T})$ and alternately sampling from the full conditional posteriors $p_\theta(x_{1:T}|y_{1:T})$ and $p(\theta|x_{1:T}, y_{1:T})$ is typically unfeasible since exact sampling from $p_\theta(x_{1:T}|y_{1:T})$ is impossible. The PG approach of Holenstein (2009) and Andrieu et al. (2010) uses an SMC algorithm targeting $\pi(x_{1:T}) = p_\theta(x_{1:T}|y_{1:T})$ in order to propose approximate samples from this distribution in such a way that the ideal Gibbs sampler is 'exactly approximated'. This is achieved by augmenting the target density of the ideal Gibbs sampler $p(\theta, x_{1:T}|y_{1:T})$ to include *all* the random variables which are produced by the SMC in order to generate an $x_{1:T}$-proposal $x^k_{1:T}$. Recall that the set of those SMC random variables is given by ($\bar{x}_{1:T}$, $\bar{a}_{1:T-1}$,k), where $\bar{x}_{1:T} = (x^1_{1:T}, \ldots, x^N_{1:T})$ denotes the N particle trajectories, $\bar{a}_{1:T-1} = (\bar{a}_1, \ldots, \bar{a}_{T-1})$ with $\bar{a}_t = (a^1_t, \ldots, a^N_t)$ the $N(T-1)$ ancestor indices generated by the resampling steps, and k the particle index drawn according to the SMC weights $\{W^i_T\}$. In order to keep track of the ancestor indices of particle $x^k_{1:T}$, we use the variable b^k_t to denote the index of the ancestor particle of $x^k_{1:T}$ at generation t. It obtains recursively as $b^k_t = k$ and $b^k_t = a^{b^k_{t+1}}_t$, and with the resulting sequence $b^k_{1:T} = (b^k_1, \ldots, b^k_T)$ we can write $x^k_{1:T} = (x^{b^k_1}_1, \ldots, x^{b^k_T}_T)$. The PG then obtains as a standard Gibbs sampler for the augmented target density over $\theta, k, \bar{x}_{1:T}, \bar{a}_{1:T-1}$.

The Gibbs sampler for this augmented target density requires a special type of SMC algorithm, referred to as *conditional* SMC, where one of the particles $\{x_{1:T}^i\}_{i=1}^N$ is specified a-priori. This pre-specified reference particle denoted by $x'_{1:T}$ is then retained throughout the entire SMC sampling process. To accomplish this, one can set $x_t^1 \equiv x'_t$ and $a_t^1 \equiv 1$ for all periods and use the SMC to sample the x_t^i's and a_t^i's only for $i = 2, ..., N$. This produces a set of N particles and IS weights $\{x_{1:T}^i, w_T^i\}_{i=1}^N$, where the first particle coincides with the pre-specified one, i.e., $x_{1:T}^1 = x'_{1:T}$ (see, e.g., Lindsten et al., 2014, Chopin and Singh, 2013).

Based on such a conditional SMC the PG algorithm for an SSM is given by:

PG algorithm

(i) *Initialization* ($j = 0$)*: Set randomly* $\theta^{(0)}$*, run an SMC targeting* $p_{\theta^{(0)}}(x_{1:T}|y_{1:T})$*, and sample* $x_{1:T}^{(0)} \sim \hat{p}_{\theta^{(0)}}(x_{1:T}|y_{1:T})$ *by drawing a particle index* k *with* $Pr(k = i) = W_T^i$ *and setting* $x_{1:T}^{(0)} = x_{1:T}^k$.

(ii) *For iteration* $j \geq 1$*:*

- *sample* $\theta^{(j)} \sim p(\theta|x_{1:T}^{(j-1)}, y_{1:T})$,
- *run a conditional SMC targeting* $p_{\theta^{(j)}}(x_{1:T}|y_{1:T})$ *conditional on* $x_{1:T}^{(j-1)}$*, and sample* $x_{1:T}^{(j)} \sim \hat{p}_{\theta^{(j)}}(x_{1:T}|y_{1:T})$ *by drawing a particle index* k *with* $Pr(k = i) = W_T^i$ *and setting* $x_{1:T}^{(j)} = x_{1:T}^k$.

The Markov kernel defined by the PG algorithm admits

$$\tilde{p}(\theta, k, \bar{x}_{1:T}, \bar{a}_{1:T-1}) = \frac{1}{N^T} p(\theta, x_{1:T}^k|y_{1:T}) \tilde{p}(\bar{x}_{1:T}^{\setminus b_{1:T}^k}, \bar{a}_{1:T-1}^{\setminus b_{1:T}^k}|x_{1:T}^k, b_{1:T}^k, \theta) \tag{9}$$

as invariant density, where $\tilde{p}$ on the r.h.s. represents the density of the random variables generated by the conditional SMC given $x_{1:T}^k, b_{1:T}^k, \theta$. Here we have used the notation $\bar{x}_{1:T}^{\setminus b_{1:T}^k}$ to denote the set on N particles $\bar{x}_{1:T}$ excluding $x_{1:T}^k$, and $\bar{a}_{1:T}^{\setminus b_{1:T}^k}$ the set of all ancestor indices excluding those associated with $x_{1:T}^k$. The specific form of this conditional density is found in Andrieu et al. (2010). The first two factors of the PG target in Equation (9) represent the marginal density of θ, $x_{1:T}^k$, $b_{1:T}^k$,

$$\tilde{p}(\theta, x_{1:T}^k, b_{1:T}^k) = \frac{1}{N^T} p(\theta, x_{1:T}^k|y_{1:T}), \tag{10}$$

defined to be the original target of interest $p(\theta, x_{1:T}^k|y_{1:T})$ up to the factor $1/N^T$ representing a discrete uniform density over the index variables in $b_{1:T}^k$. It follows that the Markov kernel defined by the PG leaves the original target $p(\theta, x_{1:T}^k|y_{1:T})$ invariant and delivers under weak regularity conditions a sequence

of draws $\{\theta^{(j)}, x_{1:T}^{(j)}\}$ whose marginal distribution converge for any $N > 1$ to $p(\theta, x_{1:T}|y_{1:T})$ as $j \to \infty$ (Andrieu et al., 2010, Theorem 5).

Existing applications of the PG use locally designed SMC algorithms like the BPF with resampling steps which are performed at every time period t. Dynamic resampling, while in principle possible, is difficult to implement and computationally inefficient since the conditional SMC at PG-iteration step j requires simulating a set of $N-1$ particles not only consistent with the retained path $x'_{1:T} = x_{1:T}^{(j-1)}$ but also with the resampling times of the SMC pass which has produced the retained path (see Holenstein, 2009, Section, 3.4.1).

3.2 Particle Gibbs and the SMC-path degeneracy

The baseline PG will, if implemented using SMCs with resampling steps at every period t, have a very poor mixing, especially, when T is large (see, Whiteley et al., 2010 and Lindsten and Schön, 2012). The reason for this is that the SMC resampling, which is used to mitigate the weight degeneracy, inevitable leads to a path degeneracy of the SMC particle system (see, e.g., Doucet and Johansen, 2009). This means that every period-t resampling step will sequentially reduce for a fixed $s < t$ and increasing t the number of unique particle values representing $x_{1:s}$, which progressively reduces the quality of the SMC samples for the path $x_{1:t}$ under $\pi_t(x_{1:t}) = p_\theta(x_{1:t}|y_{1:t})$. The consequence of this SMC path degeneracy for the PG is that at iteration step j the new trajectory $x_{1:T}^{(j)}$ tend to coalesce (for $t : T \to 1$) with the previous one $x_{1:T}^{(j-1)}$ which is retained as the reference particle $x'_{1:T}$ throughout conditional SMC sampling. Thus, the resulting particle system degenerates towards this 'frozen' path, leading to a highly dependent Markov chain.

Before we discuss in the next section solutions to this problem of the baseline PG, we emphasize two important points. First, it is not the SMC path degeneracy *per se* which leads to the poor mixing of the PG, but the degeneration of the particle system towards the retained conditional SMC reference particle $x'_{1:T}$. On the other hand, however, SMC implementations addressing successfully the path degeneracy problem can be used to fight the poor mixing of the PG. Second, by construction *any* SMC, whether implemented using locally or globally optimal IS densities, will lead to a fast degeneration of the SMC paths, when resampling is performed every period. This precludes that the mixing problem of the baseline PG resulting from the path degeneracy can be successfully addressed solely by the design of the SMC IS densities and resampling schemes.

4. Extensions of the baseline Particle Gibbs

In order to address the mixing problem of the baseline PG caused by the SMC path degeneracy the following strategies have been proposed: The first one is to augment the baseline PG by an additional particle MH update step (PGMH) proposing at each PG-iteration step j a completely new SMC path for $x_{1:T}$ (Holenstein, 2009, Section 3.2.3). The second alternative is to add additional Ancestor Sampling (AS) steps to the conditional SMC (PGAS), which assign at each time-period t a new artificial $x_{1:t-1}$-history to the partial frozen path $x'_{t:T}$ (Lindsten et al., 2014). A third strategy is to add to the conditional SMC a backward simulation step (PGBS) based on the output of the SMC forward filtering pass (Whiteley, 2010, Whiteley et al., 2010, and Lindsten and Schön, 2012). However, as discussed in Lindsten et al. (2014) this approach is in Markovian SSMs probabilistically equivalent to the PG with ancestor sampling[1].

As illustrated in our applications below the efficacy of the PGAS and PGMH to improve the mixing of the baseline PG critically depends on the SMC algorithm which is used for their implementation. In particular, an efficient PGMH implementation requires for the additional MH step numerically very precise SMC estimates of the marginal likelihood $p_\theta(y_{1:T})$, which can in high-dimensional applications be too much of a challenge for locally designed SMCs. On the other hand, the efficacy of the PGAS's ancestor sampling to improve the mixing can be seriously hampered by a large variance of the IS weights w_t^i, which is to be expected for local SMCs, especially, in SSM applications with a high signal to noise ratio (i.e., very informative observations coupled with a diffuse prior for the states). Since, as mentioned above and further detailed below, the PEIS of Scharth and Kohn (2016) uses IS densities which globally minimize across all periods the variance of the IS weights producing a very close SMC approximation to $p_\theta(x_{1:T}|y_{1:T})$ and $p_\theta(y_{1:T})$, we propose to use this PEIS in order to improve the efficiency of the PGAS and PGMH.

Moreover, the reduction of the SMC-weight degeneracy to a (close to) minimum level achieved by the PEIS, also offers the possibility to substantially reduce the SMC path degeneracy by performing the resampling step not at every but only at a few predetermined time periods (say every 500 periods). Hence, the baseline PG implemented by using the PEIS with such a sparse resampling frequency provides by itself a natural further alternative to the PGAS and PGMH in order to address the PG-mixing problem.

The extensions of the baseline PG outlined above are detailed in the next sections: In Section 4.1 we describe the PEIS. In Sections 4.2 and 4.3 we present the PGAS and PGMH, respectively, and discuss

[1]Recently, Carter et al. (2014) have extended the PGBS approach by adding in the backward simulation pass at each time period an extra MH step to generate new state values.

the potential efficiency improvements obtained if they are implemented with the PEIS.

4.1 Particle EIS (PEIS)

4.1.1 EIS principle

The PEIS as proposed by Scharth and Kohn (2016) is a 'forward-looking' SMC which uses the sequential EIS procedure of Richard and Zhang (2007) to design both IS densities and a resampling scheme. EIS is a generic algorithm which sequentially constructs a global IS density q for $x_{1:T}$ which provides a close approximation to $p_\theta(x_{1:T}|y_{1:T}) \propto p_\theta(x_{1:T}, y_{1:T})$. This global IS density is factorized conformably with $p_\theta(x_{1:T}, y_{1:T})$ in Equation (3) into

$$q(x_{1:T}; c) = \left[\prod_{t=2}^{T} q_t(x_t|x_{1:t-1}; c_t)\right] q_1(x_1; c_1), \tag{11}$$

with

$$q_t(x_t|x_{1:t-1}; c_t) = \frac{k_t(x_{1:t}; c_t)}{\chi_t(x_{1:t-1}; c_t)}, \qquad \chi_t(x_{1:t-1}; c_t) = \int k_t(x_{1:t}; c_t)dx_t, \tag{12}$$

where $\{k_t(\cdot; c_t), c_t \in \mathcal{C}_t\}$ represents a preselected class of parametric density kernels indexed by a vector of (auxiliary) parameters c_t and with known integrating factors given by χ_t. For any given $c = (c_1, ..., c_T)$ the global IS ratio $p_\theta(x_{1:T}, y_{1:T})/q(x_{1:T}; c)$ can be factorized so as to obtain

$$\frac{p_\theta(x_{1:T}, y_{1:T})}{q(x_{1:T}; c)} = \chi_1(c_1) \prod_{t=1}^{T} \left[\frac{g_\theta(y_t|x_t) f_\theta(x_t|x_{t-1}) \chi_{t+1}(x_{1:t}; c_{t+1})}{k_t(x_{1:t}; c_t)}\right], \qquad \chi_{T+1}(\cdot) \equiv 1. \tag{13}$$

In order to construct IS densities which provide a close approximation to $p_\theta(x_{1:T}, y_{1:T})$, EIS aims at selecting a value of c that minimizes the variance of this global IS ratio by minimizing period by period the variance of the individual IS ratios given in Equation (13) by the terms in brackets.

A (near) optimal value $\hat{c}$ is obtained by solving the following back-recursive sequence of least squares (LS) approximation problems:

$$(\hat{c}_t, \hat{\alpha}_t) = \arg \min_{c_t \in \mathcal{C}_t, \alpha_t \in \mathbb{R}} \sum_{i=1}^{R} \Big\{ \ln \left[g_\theta(y_t|x_t^i) f_\theta(x_t^i|x_{t-1}^i) \chi_{t+1}(x_{1:t}^i; \hat{c}_{t+1}) \right] \tag{14}$$

$$-\alpha_t - \ln k_t(x_{1:t}^i; c_t) \Big\}^2, \qquad t = T, \ldots, 1,$$

where α_t represents an intercept, and $\{x_{1:T}^i\}_{i=1}^R$ denote R independent trajectories drawn from $q(x_{1:T}; c)$

itself. Thus, $\hat{c}$ results as a fixed point solution to the sequence $\{\hat{c}^{[0]}, \hat{c}^{[1]}, \ldots\}$ in which $\hat{c}^{[\ell]}$ is obtained from (14) under trajectories drawn from $q(\cdot; \hat{c}^{[\ell-1]})$. In order to ensure convergence to a fixed-point solution it is critical that all $x_{1:T}$ draws generated for the sequence $\{\hat{c}^{[\ell]}\}$ be produced by using a single set of $T \cdot R$ canonical random numbers (CRNs) $\bar{u}_{1:T} = (u^1_{1:T}, \ldots, u^R_{1:T})$ from a density denoted by $p(\bar{u}_{1:T})$, which is typically that of uniforms or standard normals. Note that the $\hat{c}_t$'s are implicit functions of θ, so that maximal efficiency requires complete reruns of the EIS regressions for any new value of θ.

The selection of the parametric class of kernels k_t is inherently problem-specific since these kernels are meant to provide a functional approximation to the product $g_\theta(y_t|x_t)f_\theta(x_t|x_{t-1})\chi_{t+1}(x_{1:t}; c_{t+1})$. In the applications below, we consider SSMs with Gaussian transition densities f_θ, which suggest to select the k_t's as Gaussian kernels. In this case the EIS LS problems (14) take the form of simple *linear* LS problems. However, it is important to note that EIS is by no means restricted to the use of Gaussian IS samplers. The EIS LS problems become linear for all density kernels k_t chosen within the exponential family of densities and (P)EIS implementations for more flexible IS densities such as mixture of normal distributions are found in Kleppe and Liesenfeld (2014) and Scharth and Kohn (2016).

4.1.2 PEIS as an APF

The PEIS is an SMC, which is constructed from the output of this EIS algorithm as follows: Firstly, it makes use of the APF principle (Pitt and Shephard, 1999) and replaces the standard resampling scheme based upon the IS weights in Equation (8) by a scheme, which favors particles that are more likely to survive the next resampling steps. As discussed in Doucet and Johansen (2009, Section 4.2), this can be implemented within a standard SMC as outlined in Section 2.1, by replacing the natural intermediate targets $\pi_t(x_{1:t})$ in Equation (3) by auxiliary targets, which include information of future y_t-measurements. The particular auxiliary targets used by the PEIS are given by

$$\pi_t(x_{1:t}) \propto \gamma_t(x_{1:t}) \equiv p_\theta(x_{1:t}, y_{1:t})\chi_{t+1}(x_{1:t}; \hat{c}_{t+1}), \qquad \chi_{T+1}(\cdot) = 1. \tag{15}$$

Secondly, the SMC-IS densities used by the PEIS are the densities obtained from the EIS auxiliary regressions (14),

$$q_t(x_t|x_{1:t-1}) \equiv q_t(x_t|x_{1:t-1}; \hat{c}_t) = \frac{k_t(x_{1:t}; \hat{c}_t)}{\chi_t(x_{1:t-1}; \hat{c}_t)}. \tag{16}$$

Under the PEIS selections given in Equations (15) and (16), the SMC IS weights in (6) become

$$w_t^i = W_{t-1}^i \frac{g_\theta(y_t|x_t^i) f_\theta(x_t^i|x_{t-1}^i) \chi_{t+1}(x_{1:t}^i; \hat{c}_{t+1})}{k_t(x_{1:t}^i; \hat{c}_t)}. \tag{17}$$

In order to motivate this PEIS Scharth and Kohn (2016) stress that the SMC target (15) including χ_{t+1} leads to "non-standard" resampling weights that take into account the construction of the SMC IS sampling density in Equation (16) as a sequential approximation of the global target $p_\theta(x_{1:T}|y_{1:T})$. Here we complement this motivation for PEIS by providing a justification which explicitly links the factor χ_{t+1} in the auxiliary target and the PEIS sampling density q_t to the densities which they actually approximate as close as possible. Those links missing in Scharth and Kohn's motivation result from the fact that the SMC weights of the PEIS as given in Equation (17) are the weights, whose variances are sequentially minimized by the auxiliary EIS regressions (14), and are provided in the following lemma (for the proof see Appendix 1):

Lemma 1. *The factor $\chi_{t+1}(\cdot; \hat{c}_{t+1})$ as a function of $x_{1:t}$ approximates the multiperiod-a-head predictive density $p_\theta(y_{t+1:T}|x_t)$ as close as possible (up to a proportionality factor):*

$$\chi_{t+1}(x_{1:t}; \hat{c}_{t+1}) \simeq constant \cdot p_\theta(y_{t+1:T}|x_t), \tag{18}$$

and the EIS sampling density q_t approximates $p_\theta(x_t|x_{t-1}, y_{t:T})$ as close as possible:

$$q_t(x_t|x_{1:t-1}; \hat{c}_t) \simeq p_\theta(x_t|x_{t-1}, y_{t:T}). \tag{19}$$

Equation (18) implies that the intermediate SMC targets of the PEIS in Equation (15) include via the approximation of $p_\theta(y_{t+1:T}|x_t)$ a prediction about which particles will be for periods $t+1, ..., T$ in regions with high probability masses. Thus, the resulting resampling scheme based on the weights (17) favors ancestor particles with high weights in all subsequent periods. Simultaneously, the PEIS sampling densities in Equation (19) minimize according to Equations (14) and (17) the variance of the SMC-IS weights w_t^i and thus the SMC weight degeneracy across all periods. Both properties together, imply that PEIS aims at getting as close to *full global* adaption to the final target $p_\theta(x_{1:T}|y_{1:T})$ as possible, in which case the SMC IS weights would become $w_t^i \propto W_{t-1}^i \cdot 1$ for all t.

Since the PEIS implementation requires to run the sequence of T auxiliary regressions (14) *before* producing via the sequence of SMC steps a weighted particle system $\{x_{1:T}^i, w_T^i\}$, this design aiming at

perfect global adaption comes at additional computational costs relative to the local design of standard SMC procedures. However, as illustrated in our PEIS applications to PG algorithms below, the substantial improvements of the approximation to $p_\theta(x_{1:T}|y_{1:T})$ gained by the PEIS may outweigh its additional computational costs. In the following algorithm we provide a pseudo code of the PEIS.

PEIS algorithm

(i) *Draw a set of CRNs* $\bar{u}_{1:T}$ *and compute* $\hat{c} = (\hat{c}_1, \ldots, \hat{c}_T)$ *by iteratively drawing from* $q(x_{1:T}; \hat{c}^{[\ell]})$ *and producing* $c^{[\ell+1]}$ *via the* T *auxiliary EIS regressions in Equation (14), and store* $\hat{c}$.

(ii) *For* $t = 1$*:*

- *Sample* $x_1^i \sim q_1(x_1, \hat{c}_1)$*, compute the IS weights*

$$w_1^i = \frac{g_\theta(y_1|x_1^i) f_\theta(x_1^i) \chi_2(x_1^i; \hat{c}_2)}{q_1(x_1^i; \hat{c}_1)}, \tag{20}$$

store $\bar{w}_1 = \sum_{i=1}^N w_1^i/N$*, and compute normalized weights* $W_1^i = w_1^i/(\sum_{l=1}^N w_1^l)$.

- *If resampling, sample* $\bar{x}_1^i \sim \sum_{i=1}^N W_1^i \delta_{x_1^i}(dx_1)$ *and set the IS weights to* $W_1^i = 1/N$*, otherwise set* $\bar{x}_1^i = x_1^i$.

For $t = 2, ..., T$*:*

- *Sample* $x_t^i \sim q_t(x_t|\bar{x}_{1:t-1}^i, \hat{c}_t)$ *and set* $x_{1:t}^i = (x_t^i, \bar{x}_{1:t-1}^i)$*;*
- *compute the IS weights*

$$w_t^i = W_{t-1}^i \frac{g_\theta(y_t|x_t^i) f_\theta(x_t^i|x_{t-1}^i) \chi_{t+1}(x_{1:t}^i, \hat{c}_{t+1})}{k_t(x_{1:t}^i; \hat{c}_t)}, \tag{21}$$

store $\bar{w}_t = \sum_{i=1}^N w_t^i$*, and compute normalized weights* $W_t^i = w_t^i/(\sum_{l=1}^N w_t^l)$.

- *If resampling, sample* $\bar{x}_{1:t}^i \sim \sum_{i=1}^N W_t^i \delta_{x_{1:t}^i}(dx_{1:t})$ *and set the IS weights to* $W_t^i = 1/N$*, otherwise set* $\bar{x}_{1:t}^i = x_{1:t}^i$.

(iii) *If required, compute the SMC likelihood estimate according to Equation (7):*

$$\hat{z}_T = \hat{p}_\theta(y_{1:T}) = \chi_1(\hat{c}_1) \prod_{t=1}^T \bar{w}_t. \tag{22}$$

As discussed above, PEIS differs from standard SMCs such as BPF and APF by its forward-looking design incorporating information in the data $y_{t:T}$ into the targets $\pi(x_{1:t})$ and sampling densities q_t. A further difference is that in PEIS the parameters of the targets and sampling densities are, in contrast to standard SMCs, random variables since they depend via the optimal EIS auxiliary parameters $\hat{c}$ on the

EIS CRNs $\bar{u}_{1:T}$ (see step (i) of the PEIS algorithm). However, the future data $y_{t:T}$ is fixed as it is also the case for the EIS parameters $\hat{c}$ when it comes to generating the SMC particles $\bar{x}_{1:T}$ and ancestor indices $\bar{a}_{1:T-1}$ in step (ii) of the PEIS algorithm. With fixed $y_{t:T}$ and $\hat{c}$ neither the forward-looking design nor the dependence of $\hat{c}$ on the CRNs $\bar{u}_{1:T}$ changes the inherent structure in the joint distribution of the SMC particles $\bar{x}_{1:T}$ and ancestor indices $\bar{a}_{1:T-1}$ defined by a standard SMC or its conditional SMC counterpart required by PG. It follows that conditional on $\bar{u}_{1:T}$ the PEIS defines a valid SMC representing a special case of the generic SMC algorithm for the PMCMC framework of Andrieu et al. (2010). Also it produces by $\hat{p}_\theta(y_{1:T})$ in Equation (22) unbiased estimates of the likelihood $p_\theta(y_{1:T})$ (Scharth and Kohn, 2016).

4.1.3 PG with PEIS

Since PEIS defines conditional on the EIS CRNs a valid SMC, we can suggest to use it in the PG algorithm in Section 3.1. For the validity of the resulting PG-PEIS procedure, however, it is critical that we include those CRNs into the PG Markov kernel. This can be easily implemented by drawing in each PG sweep j a new set of CRNs $\bar{u}_{1:T}^{(j)}$ to produce via the initial EIS regressions (14) the auxiliary parameters $\hat{c}^{(j)}$ for the PEIS version of the conditional SMC step targeting $p_{\theta^{(j)}}(x_{1:T}|y_{1:T})$. It follows that such an PG-PEIS procedure defines a Markov kernel including updates for the CRNs $\bar{u}_{1:T}$, and the corresponding target density obtains as the following straightforward extension of the PG target in Equation (9):

$$\tilde{p}(\theta, k, \bar{x}_{1:T}, \bar{a}_{1:T-1}, \bar{u}_{1:T}) = \frac{1}{N^T} p(\theta, x_{1:T}^k|y_{1:T}) p(\bar{u}_{1:T}) \tilde{p}(\bar{x}_{1:T}^{\setminus b_{1:T}^k}, \bar{a}_{1:T-1}^{\setminus b_{1:T}^k}|x_{1:T}^k, b_{1:T}^k, \theta, \bar{u}_{1:T}), \tag{23}$$

where $p(\bar{u}_{1:T})$ is the canonical density of the EIS CRNs. The function $\tilde{p}$ on the r.h.s represents the density of the random variables generated by the conditional PEIS given $\theta, x_{1:T}^k, b_{1:T}^k, \hat{c}$, where we can replace $\bar{u}_{1:T}$ by $\hat{c}$ since $\hat{c}$ given θ obtains via the EIS regressions (14) as a deterministic function of $\bar{u}_{1:T}$. Note that the updating step for $\bar{u}_{1:T}$ consists of drawing from its marginal density $p(\bar{u}_{1:T})$, which implies that $\bar{u}_{1:T}$ is marginalized out in the individual Gibbs sweeps. But this marginalization leaves the extended target density $\tilde{p}(\theta, k, \bar{x}_{1:T}, \bar{a}_{1:T-1}, \bar{u}_{1:T})$ invariant (Liu, 1994). Moreover, the extended target (23) includes in the same way as the PG target in Equation (9) the original target density $p(\theta, x_{1:T}^k|y_{1:T})$ as a marginal. It follows that the augmented Markov kernel defined by the PG-PEIS leaves $p(\theta, x_{1:T}^k|y_{1:T})$ invariant. Note also that since $\hat{c}$ given θ is a deterministic function of $\bar{u}_{1:T}$, the augmentation of the original PG kernel by $\bar{u}_{1:T}$ represents basically an extension of a Markov kernel to include random (auxiliary) tuning parameters for an MCMC proposal density, which is a well-established approach (Zhang and Sutton, 2011, Kleppe,

2016, Lindsten and Doucet, 2016).

As discussed above, the PEIS when implemented with SMC-resampling steps in every period will suffer, as any SMC, from the SMC-path degeneracy phenomenon causing the poor mixing of the baseline PG. Hence, we can not expect that such a brute-force PG-PEIS implementation will satisfactorily address the poor mixing problem of PG. However, since the PEIS globally reduces the variance of the SMC-IS weights to a (close to) minimum level, it typically suffices to resample only at a few periods, which substantially reduces the path degeneracy. This motivates the implementation of the baseline PG using the PEIS with sparse resampling at a few predetermined time period (PG-PEIS-sparse). Moreover, the PG-PEIS framework allows us to improve the PG extensions which we discuss next.

4.2 Particle Gibbs with ancestor sampling (PGAS)

In order to address the poor mixing of the baseline PG, Lindsten et al. (2014) developed the PGAS. It exploits the fact that it suffices to suppress the degeneration of the particle system towards the retained conditional SMC reference trajectory $x'_{1:T}$ and not the SMC-path degeneracy per se to improve the mixing. Based on this insight, the basic idea of the PGAS is to break this reference trajectory into pieces, so that the particle system tends to degenerate to something different than the reference trajectory.

In particular, the PGAS augments each period-t conditional-SMC resampling step by randomly selecting from the set $\{x^i_{1:t-1}\}_{i=1}^N$ (including the reference particle $x'_{1:t-1}$) one ancestor particle which is used to assign a potentially new $x_{1:t-1}$-history to the partial frozen path $x'_{t:T}$. This produces a concatenated full path $[x^i_{1:t-1}, x'_{t:T}]$, and the corresponding (non-normalized) weight for selecting $x^i_{1:t-1}$ as the new ancestor for $x'_{t:T}$ is given by

$$\tilde{w}^i_{t-1|T} = w^i_{t-1} \frac{\gamma_T\left([x^i_{1:t-1}, x'_{t:T}]\right)}{\gamma_{t-1}(x^i_{1:t-1})}. \tag{24}$$

In Bayesian terms, the components of those anchestor sampling weights for the reference particle are the prior probability of the ancestor particle $x^i_{1:t-1}$ given by the 'standard' SMC-IS weights w^i_{t-1} and the likelihood that the partial reference path $x'_{t:T}$ originated from $x^i_{1:t-1}$ which is represented by the ratio of the targets $\gamma_T(\cdot)/\gamma_{t-1}(\cdot)$.

As shown by Lindsten et al. (2014, Theorem 1), the invariance property of the baseline PG is not violated by this additional AS step. However, since this AS step sequentially assigns in each period a potentially new ancestor to $x'_{t:T}$, it will produce a reference path $x'_{1:T}$ which tends to differ from the other (degenerated) conditional SMC paths $\{x^i_{1:T}\}_{i=2}^N$. Thus, while not preventing the particle system

to degenerate, the PGAS typically improves the mixing of the baseline PG. Furthermore, if the variance of the AS weights $\tilde{w}^i_{t-1|T}$ in Equation (24) is minimized, the potential diversity of the resulting PGAS reference path $x'_{1:T}$ is maximized. Hence, by reducing the variance of $\tilde{w}^i_{t-1|T}$, we can improve the mixing of the PGAS trajectories $x^{(j)}_{1:T}$ under $p_\theta(x_{1:T}|y_{1:T})$.

In Lindsten et al. (2014), the PGAS is implemented by relying upon the BPF (PGAS-BPF), which uses $\pi_t(x_{1:t}) \propto p_\theta(x_{1:t}, y_{1:t})$, as given in Equation (3), together with $q_t(x_t|x_{1:t-1}) \equiv f_\theta(x_t|x_{t-1})$, so that according to Equation (6) the 'prior' weights are $w^i_{t-1} = W^i_{t-2} g_\theta(y_{t-1}|x^i_{t-1})$. The resulting AS weights are given by

$$\tilde{w}^i_{t-1|T} = W^i_{t-2} g_\theta(y_{t-1}|x^i_{t-1}) p_\theta(x'_{t:T}, y_{t:T}|x^i_{t-1}) \propto W^i_{t-2} g_\theta(y_{t-1}|x^i_{t-1}) f_\theta(x'_t|x^i_{t-1}). \tag{25}$$

This form of AS-weights obtained under the BPF, shows that in scenarios, where the measurement density g_θ is fairly flat in x_t (so that the y_t observations are not very informative about the states x_t) and the transition density f_θ exhibits a large conditional variance, the variation of $\tilde{w}^i_{t-1|T}$ can be expected to be sufficiently small so as to obtain a sufficiently strong mixing of the PGAS-BPF. However, applications with highly informative observations and/or a state process with small noise produce a large variance of $\tilde{w}^i_{t-1|T}$, so that the efficacy of the PGAS-BPF to improve the mixing of the baseline PG can be expected to be limited.

Under the PEIS with $\pi_t(x_{1:t})$ and w^i_{t-1} as given by Equations (15) and (17) the PGAS ancestor weights become

$$\tilde{w}^i_{t-1|T} \quad \propto \quad \left[W^i_{t-2} \frac{g_\theta(y_{t-1}|x^i_{t-1}) f_\theta(x^i_{t-1}|x^i_{t-2}) \chi_t(x^i_{1:t-1}; \hat{c}_t)}{k_{t-1}(x^i_{1:t-1}; \hat{c}_{t-1})} \right] \left[\frac{p_\theta(y_{t:T}|x^i_{t-1})}{\chi_t(x^i_{1:t-1})} \right]. \tag{26}$$

Hence, according to Lemma 1 the PEIS produces PGAS ancestor weights with a (close to) minimal variation: Recall that the IS densities of the PEIS are designed so as to minimize the variance of the prior weights w^i_{t-1} (given by the term in the first bracket of Equation 26). Moreover, the predictive density $p_\theta(y_{t:T}|x_{t-1})$ as function in x_{t-1} is closely approximated by the EIS integrating factor $\chi_t(x_{1:t-1})$ so that the variance of the likelihood for the ancestor $x^i_{1:t-1}$ (term in the second bracket) is also close to a minimum level. In other words, the PEIS not only produces a (conditional) SMC particle system which is nearly perfectly globally adapted to $p_\theta(x_{1:T}|y_{1:T})$, but also generates a very high potential diversity of the reference particle generated by the additional AS step. As a result, we expect to improve the mixing of the PGAS paths for $x_{1:T}$ obtained under local procedures like the BPF by relying upon the global PEIS

(PGAS-PEIS).

As to the validity of the PGAS-PEIS, we note that Theorem 1 in Lindsten et al. (2014) establishing the invariance property of the PGAS kernel is not affected by the use of PEIS. In fact, when using the PEIS this invariance property of the PGAS holds true conditional on the EIS CRNs $\bar{u}_{1:T}$ so that we can augment the PGAS kernel in line with with the augmentation discussed in Section 4.1.3 to include the (marginal) update steps for $\bar{u}_{1:T}$ which preserve the invariance.

4.3 Particle Gibbs with an additional MH step (PGMH)

The PGMH proposed by Holenstein (2009, Algorithm 3.6) in order to address the poor-mixing problem of the baseline PG bypasses the SMC-path degeneracy by using an additional particle-MH step proposing in each iteration step j a completely new SMC path denoted by $x^*_{1:T}$. This new path is MH-compared with the old path $x^{(j-1)}_{1:T}$ based upon the (conditional) SMC estimates of their respective marginal likelihood. The resulting PGMH algorithm is given by:

PGMH algorithm

(i) *Initialization* ($j = 0$)*: Set randomly* $\theta^{(0)}$*, run an SMC targeting* $p_{\theta^{(0)}}(x_{1:T}|y_{1:T})$*, and sample* $x^{(0)}_{1:T} \sim \hat{p}_{\theta^{(0)}}(x_{1:T}|y_{1:T})$.

(ii) *For iteration* $j \geq 1$*:*

- *sample* $\theta^{(j)} \sim p(\theta|x^{(j-1)}_{1:T}, y_{1:T})$,
- *run a conditional SMC targeting* $p_{\theta^{(j)}}(x_{1:T}|y_{1:T})$ *conditional on* $x^{(j-1)}_{1:T}$*, and compute the likelihood estimate* $\hat{p}_{\theta^{(j)}}(y_{1:T})$*,*
- *run an SMC targeting* $p_{\theta^{(j)}}(x_{1:T}|y_{1:T})$*, sample* $x^*_{1:T} \sim \hat{p}_{\theta^{(j)}}(x_{1:T}|y_{1:T})$*, and compute the likelihood estimate* $\hat{p}^*_{\theta^{(j)}}(y_{1:T})$*,*
- *with probability*

$$1 \wedge \frac{\hat{p}^*_{\theta^{(j)}}(y_{1:T})}{\hat{p}_{\theta^{(j)}}(y_{1:T})} \tag{27}$$

set $x^{(j)}_{1:T} = x^*_{1:T}$*, otherwise* $x^{(j)}_{1:T} = x^{(j-1)}_{1:T}$.

The efficacy of this PGMH algorithm to improve the mixing of the baseline PG critically depends on the numerical precision of the (conditional) SMC estimates for the marginal likelihood $p_\theta(y_{1:T})$ defining the acceptance rate of the additional particle MH-step as given in Equation (27). In particular, if the SMC delivers noisy estimates for $p_\theta(y_{1:T})$ the MH updates for $x_{1:T}$ can get stuck for many iterations leading

to very poor mixing. Hence, efficient PGMH implementations are those for which the SMC marginal likelihood estimates have a small variance. Since, as discussed in Section 4.1, the PEIS produces very precise SMC estimates, we expect a high efficacy of the PGMH in improving the mixing of the baseline PG by relying upon PEIS estimates for $p_\theta(y_{1:T})$ as given by Equation (22) (PGMH-PEIS).

Note that this PGMH-PEIS algorithm implemented with redrawing in each sweep j the EIS-CRNs $\bar{u}_{1:T}$ has the desired invariant distribution, which follows directly from the target-augmentation principle discussed in Section 4.1.3 and the fact that the PEIS SMC estimation for the marginal likelihoods in Equation (27) is unbiased (Scharth and Kohn, 2016).

5. Univariate Applications

In this section we discuss two univariate applications illustrating how the PEIS can be used to improve the mixing of the baseline PG and its PGAS and PGMH extensions. The examples are designed to illustrate the relative performance of PG-PEIS implementations under different empirically relevant scenarios. Later in Section 6 we present a multivariate application to show the effectiveness of the PG-PEIS strategy in state space models with high-dimensional latent state vectors, where the PG framework allows us to decompose the high dimensional problem into simpler, lower dimensional ones.

5.1 Example Models

The first example is a standard stochastic volatility (SV) model for the volatility of financial returns (see, e.g., Ghysels et al., 1996). It has the form

$$y_t = \beta \exp\{x_t/2\}\eta_t, \qquad \eta_t \sim \text{i.i.d.} N(0,1), \tag{28}$$

$$x_t = \delta x_{t-1} + \nu\epsilon_t, \qquad \epsilon_t \sim \text{i.i.d.} N(0,1), \tag{29}$$

where y_t is the asset return observed at period t, x_t is the latent log volatility and $\theta = (\beta, \delta, \nu)'$. The innovations ϵ_t and η_t are mutually independent. Assuming $|\delta| < 1$, the distribution of the initial state is given by $x_1 \sim N(0, \nu^2/[1-\delta^2])$.

The second example is a time-discretized version of a constant elasticity of variance (CEV) diffusion model for daily short-term interest rates (Chan et al., 1992). In order to account for microstructure noise, which is to be expected for interest rate data at the daily frequency, the basic CEV specification is

extended to include a noise component (Aït-Sahalia, 1999 and Kleppe and Skaug, 2015). The resulting model for the interest rate y_t observed at day t with x_t the latent interest-rate state, is described as

$$y_t = x_t + \sigma_y \eta_t, \qquad \eta_t \sim \text{i.i.d.} N(0,1), \tag{30}$$

$$x_t = x_{t-1} + \Delta(\alpha - \beta x_{t-1}) + \sigma_x x_{t-1}^{\gamma} \sqrt{\Delta} \epsilon_t, \qquad \epsilon_t \sim \text{i.i.d.} N(0,1), \tag{31}$$

where ϵ_t and η_t are independent and $\Delta = 1/252$. The parameters are $\theta = (\alpha, \beta, \sigma_x, \gamma, \sigma_y)'$. As the stationary distribution of x_t is not known analytically, we assume for the initial state x_1 a normal distribution with a mean set equal to the observed value of y_1 and a standard deviation of 100 basis points so that $x_1 \sim N(y_1, [0.01]^2)$.

The data we use for the SV model are daily log returns, multiplied by 100, of the S&P 500 stock index from October 1, 1999 to September 30, 2009, with a sample size of $T = 2515$. The data for the CEV model consists of daily 7-day Eurodollar deposit spot rates from January 2, 1983 to February 25, 1995, with $T = 3082$. (This data set is discussed in more detail in Aït Sahalia, 1996). See Figure 1 for time series plots of the SV and CEV data.

The two example models differ in their statistical structure and pose different challenges to PG algorithms. The SV model involves a linear Gaussian transition density and a measurement density which is non-Gaussian in the states. In the SV return data the parameter estimates imply a measurement density which is not very informative about the states and state innovations which are fairly volatile. This represents a scenario, where standard SMCs typically exhibit a satisfactory performance. In the CEV model we have a nonlinear Gaussian state transition density f_θ coupled with a measurement density g_θ which is Gaussian in the states. In the interest data for this model, the estimated standard deviation of the measurement error σ_y we obtain is small relative to the typical standard deviation of the state innovations $\sigma_x x_{t-1}^{\gamma} \sqrt{\Delta}$, so that the observations are much more informative about the states than in the SV model. This leads to a large sensitivity of SMC procedures to outliers (see, e.g., DeJong et al., 2013) with potential adverse effect on the efficiency of the PG. Such outliers are frequently observed in interest rate data.

5.2 PEIS implementation

As discussed in Section 4.1, the implementation of (P)EIS requires to select a parametric class for the EIS density kernel $k_t(x_{1:t}, c_t)$ capable of providing a good functional approximation to the period-t EIS

target given by (see Equation 13)

$$g_\theta(y_t|x_t)f_\theta(x_t|x_{t-1})\chi_{t+1}(x_{1:t};c_{t+1}). \tag{32}$$

Both example models have in common that they involve a Gaussian transition density with a conditional mean μ_t and variance σ_t^2, written as $f_\theta(x_t|x_{t-1}) = f_N(x_t|\mu_t,\sigma_t^2)$, where for the SV model we have $\mu_t = \delta x_{t-1}$ and $\sigma_t^2 = \nu^2$, while for the CEV model it is the case that $\mu_t = x_{t-1}+\Delta(\alpha-\beta x_{t-1})$ and $\sigma_t^2 = \sigma_x^2 x_{t-1}^{2\gamma}\Delta$.

In such Gaussian transition cases it is natural to select for k_t a Gaussian kernel in x_t which consists of the product of the Gaussian transition density f_θ already included in the EIS target in Equation (32) and a Gaussian kernel approximation in x_t to the remaining non-Gaussian product $g_\theta\,\chi_{t+1}$. The corresponding EIS kernel k_t can be parameterized as

$$k_t(x_{1:t},c_t) = f_\theta(x_t|x_{t-1})\zeta_t(x_t;c_t), \quad \text{with} \quad \zeta_t(x_t;c_t) = \exp\{c_{1t}x_t + c_{2t}x_t^2\}, \tag{33}$$

where ζ_t is the Gaussian kernel designed to approximate $g_\theta\,\chi_{t+1}$ with auxiliary EIS parameters $c_t = (c_{1t},c_{2t})$. Since f_θ in the kernel k_t as defined in Equation (33) is also a component of the EIS target, it cancels out in the EIS regressions (14). Hence, they simplify into simple linear LS regressions of $\ln[g_\theta(y_t|x_t^i)\chi_{t+1}(x_{1:t}^i;\hat{c}_{t+1})]$ on x_t^i and $(x_t^i)^2$ and a constant.

From Equation (33) it immediately follows that the Gaussian EIS density for $x_t|x_{t-1}$ has the form

$$q_t(x_t|x_{t-1},c_t) = f_N\left(x_t|m_t,v_t^2\right), \quad \text{with} \quad v_t^2 = \frac{\sigma_t^2}{1-2c_{2t}\sigma_t^2}, \quad m_t = v_t^2\left(\frac{\mu_t}{\sigma_t^2}+c_{1t}\right), \tag{34}$$

and integrating k_t w.r.t. x_t leads to the following integrating factor:

$$\chi_t(x_{1:t-1},c_t) = \frac{\sqrt{v_t^2}}{\sqrt{\sigma_t^2}}\exp\left\{\frac{1}{2}\left(\frac{m_t^2}{v_t^2}-\frac{\mu_t^2}{\sigma_t^2}\right)\right\}. \tag{35}$$

As mentioned in Section 4.1, the sequence of EIS regressions in Equation (14) producing near optimal values for the EIS parameters c need to be iterated since the R trajectories $\{x_{1:T}^i\}_{i=1}^R$ used in the EIS regression are to be drawn from the joint IS density $q(x_{1:T};c)$ itself. This requires selecting an initial value $\hat{c}^{[0]} = (\hat{c}_1^{[0]},...,\hat{c}_T^{[0]})$ and then for iteration $\ell = 1,...,L$ using trajectories from $q(x_{1:T};\hat{c}^{[\ell-1]})$ to compute a new $c^{[\ell]}$. Actually, when using a number of EIS trajectories R of the order of 3 to 5 times the number of parameters in the period-t EIS regression, only the first 2 or 3 iterations produce significant improvements

on the approximation of the EIS targets as measured by the R^2 of the EIS LS regressions. Thus we preset the number of EIS iterations at $L = 4$ and set $R = 15$. As for $\hat{c}^{[0]}$, we can exploit that in the case of the CEV model the measurement density $g_\theta(y_t|x_t)$ in the EIS targets itself is a Gaussian kernel in x_t so that we can select $\hat{c}_t^{[0]}$ as that value for c_t for which $\zeta_t(x_t; c_t) \propto g_\theta(y_t|x_t)$. It follows that the resulting initial EIS density $q_t(x_t|x_{t-1}, \hat{c}_t^{[0]})$ corresponds to the IS density of the conditional optimal particle filter. For the SV model, $g_\theta(y_t|x_t)$ is non-Gaussian in x_t so that we use for $\ln \zeta_t$ a second-order Taylor-series approximation in x_t to $\ln g_\theta$ to obtain an initial value $\hat{c}_t^{[0]}$. The R^2 we find in the final sequence of EIS regressions is typically larger than 0.99, which indicates that the resulting EIS densities are nearly perfectly globally adapted to the SMC target $p_\theta(x_{1:T}|y_{1:T})$.

The functional forms of the EIS densities given in Equations (33) to (35) together with the near optimal value $\hat{c} = \hat{c}^{[L]}$ are used to run the SMC steps (ii) and (iii) of the PEIS algorithm provided in Section 4.1. Note that this PEIS algorithm covers the standard BPF as a special case with $\hat{c} \equiv 0$, leading to $k_t(x_{1:t}; 0) = f_\theta(x_t|x_{t-1})$ with $\chi_t(x_{1:t-1}; 0) = 1$.

5.3 Results

Here we present simulation experiments using the SV and CEV model to compare the following 8 PG schemes:[2] The baseline PG based on the BPF (PG-BPF), PEIS (PG-PEIS) and PEIS with sparse resampling (PG-PEIS-sparse), then the PGAS combined with the BPF (PGAS-BPF) and PEIS (PGAS-PEIS) and, finally, the PGMH using the BPF (PGMH-BPF), PEIS (PGMH-PEIS) and PEIS-sparse (PGMH-PEIS-sparse). We use multinomial resampling for the SMC resampling steps. For the PEIS-sparse the resampling is conducted only every 500 periods. The PG methods were all implemented in the interpreted language MATLAB, making computing times comparable.

For all the experiments we use the real data sets described in Section 5.1. The corresponding maximum likelihood (ML) estimates based on EIS evaluations of the likelihood are $(\beta, \delta, \nu) = (1.065, 0.992, 0.122)$ for the SV model and $(\alpha, \beta, \sigma_x, \gamma, \sigma_y) = (0.0097, 0.1656, 0.4250, 1.201, 0.0005)$ for the CEV model.

[2] In addition, for the CEV model we considered the PGAS based on the fully adapted APF, which extends the intermediate target in Equation (3) by including the one-period ahead predictive density $p_\theta(y_{t+1}|x_t)$ and uses the conditional optimal IS density $p_\theta(x_t|y_t, x_{t-1})$ (see, Pitt et al., 2012, and Pitt et al., 2015). However, the results are not reported here as the predictive density and the conditional optimal IS density are analytically known only for the CEV model but not for the SV application. Moreover, the PGAS results for the CEV model show no improvements when replacing the BPF by the fully adapted APF.

5.3.1 Mixing of Particle Gibbs for fixed parameters

The first experiment is designed to analyze the mixing of the PG algorithms w.r.t. the states under their joint posterior $p_\theta(x_{1:T}|y_{1:T})$ for a fixed value of the parameters θ. Throughout this experiment we set the parameters equal to their ML estimates and generate samples from this density using the PG algorithms, which are all implemented with two different numbers of particles, $N = 30$ and $N = 1000$. All methods are simulated for 1100 iterations, where the first 100 burn-in iterations are discarded.

In order to compare the mixing, we follow Lindsten et al. (2014) and compute the update rate for each x_t $(t = 1, ..., T)$ which is defined as the proportion of PG iterations where the value for x_t has changed. The update rates for the 8 PG algorithms plotted against time t are provided in Figure 2 for the SV model and in Figure 3 for the CEV model. They reveal that in both example models the update rate for the baseline PG-BPF for $N = 30$ as well as $N = 1000$ rapidly decreases for an increasing distance of t to the final period T. These poor update rates reflect the typical SMC path degeneracy causing, as discussed in Section 4.2, the state trajectory $x_{1:T}^{(j)}$ at PG iteration step j to coalesce with the previous trajectory $x_{1:T}^{(j-1)}$. That this poor mixing problem cannot be addressed satisfactorily by replacing the locally designed BPF by an SMC which is nearly perfectly globally adapted is evidenced by the update rates of the PG-PEIS: Even if they increase relative to the PG-BPF they fall in both models, even with $N = 1000$ particles, below 20% for the states of the first 500 periods. This is an illustration of the 'unavoidable' SMC path degeneracy which we would obtain under a fully optimal SMC when resampling is performed every period. The update rates for the PG-PEIS-sparse remaining above 70% across all periods show that, as expected, sparse resampling greatly improves the mixing of the PG-PEIS by reducing the path degeneracy.

The comparison of the baseline PG-BPF with the PGAS-BPF shows that the additional AS step also increases significantly the average probability of updating x_t across all periods which is consistent with the results reported by Lindsten et al. (2014). However, for the CEV model, in particular, this probability drops dramatically in many periods, indicating that in these periods very few particles tend to keep all the weights across the PG iterations. As discussed in Section 4.2, this stems from the model's tight measurement distribution which makes the PGAS particularly vulnerable to outliers as they produce AS weights with a large variance (see Equation, 25). This effect appears to be less acute for the SV model reflecting the fact that its measurement distribution is not very sensitive to the state. When combined with PEIS, the PGAS with as little as $N = 30$ particles produce update rates which are uniformly above 95% for both, the CEV model and the SV model, indicating a close to perfect and robust mixing of the

PGAS.

Turning to the PG augmented by an additional MH move, we also find in both example models a substantial improvement in the mixing when replacing the BPF by PEIS or PEIS-sparse. Those improvements reflect the fact that, as discussed in Section 4.3, PEIS(-sparse) produce numerically far more accurate SMC estimates of the marginal likelihood than the BPF.

For a further comparison of the PG methods, we compute the effective sample size (ESS) of the posterior samples for the state variable x_t at each time period t. The ESS is defined as

$$\text{ESS} = M \left[1 + 2\sum_{j=1}^{J} \gamma(j)\right]^{-1}, \tag{36}$$

where M is the size of the posterior sample, and $\sum_j \gamma(j)$ the sum of the J monotone sample autocorrelations as estimated by the initial monotone sequence estimator proposed by Geyer (1992). The interpretation is that the M PG draws lead to the same precision as a hypothetical i.i.d. sample from the posterior of size ESS, so that large values for ESS are preferable. We consider the minimum, median and maximum ESS over the T sampled state variables. These ESS values are computed for 10 independent complete PG runs from which we take the corresponding averages. In order to account for different computing times, we also compute the (average) minimum ESS standardized by the Central Processor Unit (CPU) time required to run a PG algorithm. It measures the time it takes to obtain one i.i.d. draw of the *complete* $x_{1:T}$-trajectory from its posterior. The ESS results are reported in Table 1 for the SV model and in Table 2 for the CEV model.

The results for both models show that, for a given number of particles N, the PEIS(-sparse) substantially increases the median and the minimum ESS of the baseline PG, PGAS and PGMH relative to their corresponding BPF counterpart. The largest i.i.d. sample from $p_\theta(x_{1:T}|y_{1:T})$ per hour computing time is produced by the PG-PEIS-sparse with $N = 1000$ for the SV model, and by the PGAS-PEIS with $N = 30$ for the CEV model. This illustrates that the improvements of the PG approximations to $p_\theta(x_{1:T}|y_{1:T})$ gained by the global PEIS outweigh its additional computational costs relative to the locally designed BPF.

5.3.2 Full Bayesian analysis

Here, we compare the performance of the PG algorithms for a full Bayesian analysis of the two example models. For the parameters of both models we select fairly uninformative priors (for details of the prior

selection, see Appendix 2). In light of the severe mixing problems of the PG-BPF, PG-PEIS and PGMH-BPF documented in the previous section, the remainder investigation focuses on the efficiency of the PG-PEIS-sparse, PGAS-BPF, PGAS-PEIS, PGMH-PEIS and PGMH-PEIS-sparse. For all of those five methods we use throughout 50,000 PG iterations where the first 10,000 burn-in iterations are discarded.

The Bayesian posterior results for the five PG procedures, each based on $N = 30$ particles, are summarized in Table 3 for the SV model and in Table 4 for the CEV model. Both tables report the following statistics for the model parameters (θ), the initial (x_1), middle ($x_{T/2}$) and last state (x_T): The PG posterior mean and standard deviation together with the ESS and ESS standardized by computing time. All statistics reported in Tables 3 and 4 are sample averages which are computed from 10 independent replications obtained by running each of the PG algorithms under 10 different seeds. The tables also provide the corresponding statistics for the 'ideal' Gibbs sampler, i.e., the sampler which simulates $x_{1:T}$ directly from the true posterior $p_\theta(x_{1:T}|y_{1:T})$. This fictitious Gibbs sampler is approximated by the PGAS-PEIS implemented with $N = 10,000$ particles. Since the PG algorithms can be seen as MC approximations of the ideal Gibbs sampler, the latter provides a natural benchmark for the mixing performance of the former (see, e.g., Lindsten et al. 2014).

From the results for the SV model in Table 3 we see that with $N = 30$ all five PG algorithms produce MC estimates of the posterior means which are close to those of the ideal Gibbs sampler and the corresponding ML estimates. The ESS values indicate that replacing the BPF by PEIS improves, as expected from the results in Section 5.3.1, the mixing of the PGAS for the parameters and states, and shifts the ESS values closer to those of the ideal Gibbs sampler. The remaining PG-schemes based upon PEIS or PEIS-sparse also show a satisfactory mixing relative to the ideal Gibbs. Most critical for a posterior Gibbs analysis of the parameters θ appears to be the scaling parameter β, which has among all parameters and across all PG procedures the smallest ESS value. Hence, the mixing of the sampled β's sets the limit w.r.t. the amount of i.i.d. draws for θ which can be generated for a given number of Gibbs iterations or a fixed computing time. In terms of the largest minimum ESS of the sampled parameters per hour computing time, the PG-PEIS-sparse and PGAS-BPF show the best performance. For $N = 30$ particles both produce per hour 7 i.i.d. draws from the marginal posterior of the parameters $p(\theta|y_{1:T})$.

In order to analyze the robustness of the PG procedures w.r.t. the selected number of particles, we plot in Figure 4 the autocorrelation functions (ACF) of the sampled β-parameter for the PGAS-BPF and PGAS-PEIS for a range of different number of particles N. The ACF plots reveal that the PEIS version of the PGAS produce comparable mixing rates for any number of particles N larger than 30, suggesting

that it does not require more than $N = 30$ particles to obtain a performance which comes close to that of the ideal Gibbs. In contrast, for the BPF counterpart to achieve this performance it needs more than $N = 100$ particles.

Turning to the PG posterior results for the CEV model in Table 4, we first note that the MC estimates for the posterior mean of the parameters θ associated with the PG procedures based on PEIS are all in close agreement with those of the ideal Gibbs and their ML counterparts. For the PGAS based on BPF, however, the posterior parameter estimates substantially differ from those benchmarks. These serious biases are consistent with the results of Section 5.3.1, showing that in situations involving tight measurement densities coupled with outliers the PGAS-BPF has severe problems to fully explore the domain of the states under $p_\theta(x_{1:T}|y_{1:T})$. That the measurement density in this example is fairly tight is indicated by the tiny value of the estimates for the standard deviation σ_y. In contrast to the PGAS-BPF, the PG procedures based on PEIS ensure even in this challenging scenario a fast and reliable exploration of $p_\theta(x_{1:T}|y_{1:T})$ and lead to accurate posterior estimates for the parameters. Note also that the ESS values in Table 4 indicate that with $N = 30$ particles the mixing rate of all PG procedures using PEIS is very close to that of the ideal Gibbs sampler. (Since the PGAS-BPF parameter draws apparently fail to appropriately represent the posterior $p(\theta|y_{1:T})$ we refrain from reporting the corresponding values of the ESS statistic.)

The two parameters with the lowest ESS values are σ_x and γ. In Figure 4 we plot the ACF for those two parameters sampled by the PGAS-PEIS under different number of particles. The results reveal that the PGAS-PEIS achieves a performance close to that of an ideal Gibbs with as little as $N = 5$ particles.

6. Multivariate Application

6.1 Model

We now turn to a multivariate example where we consider the multivariate stochastic volatility model of Tsay (2010, Section 12.7.2) adapted to the modelling of the realized covariance matrices observed for a set of q asset returns (for a discussion of realized covariances, see Barndorff-Nielsen and Shephard, 2004). For the $q \times q$ realized covariance matrix Y_t we assume an inverted Wishart distribution $IW_q(\nu, \Sigma_t)$ with density

$$g_\theta(Y_t|\Sigma_t) = \frac{|\Sigma_t|^{\nu/2}|Y_t|^{-(\nu+q+1)/2}\exp\{-(1/2)\mathrm{tr}(\Sigma_t Y_t^{-1})\}}{2^{\nu q/2}\pi^{q(q-1)/4}\prod_{\ell=1}^{q}\Gamma([\nu+1-\ell]/2)}, \tag{37}$$

where Σ_t is the period-t positive definite $q \times q$ scale matrix and $\nu > q+1$ the degrees of freedom so that $E(Y_t|\Sigma_t) = \Sigma_t/(\nu - q - 1)$ (Anderson, 1984, Jin and Mahieu, 2016). The time-varying scale matrix Σ_t directing the conditional mean of the realized (co)variances is Cholesky-decomposed and is taken to depend upon a latent Gaussian autoregressive state vector $x_t = (x_{1t}, ..., x_{qt})$ in the form

$$\Sigma_t = H D_t H', \quad D_t = \text{diag}\{\exp(x_{1t}), \ldots, \exp(x_{qt})\}, \tag{38}$$

$$x_{\ell t} = \mu_\ell + \delta_\ell(x_{\ell t-1} - \mu_\ell) + \sigma_\ell \epsilon_{\ell t}, \quad \epsilon_{\ell t} \sim \text{i.i.d.} N(0,1), \quad \ell = 1, \ldots, q, \tag{39}$$

where $x_{\ell 1} \sim N(\mu_\ell, \sigma_\ell^2/[1-\delta_\ell^2])$. The matrix H is a lower-triangular $q \times q$ parameter matrix with unit diagonal elements. Its column vectors denoted by h_ℓ ($\ell = 1, \ldots, q$) have the form $h_\ell = (0, \ldots, 0, 1, \tilde{h}_\ell')'$, where $\tilde{h}_\ell = (\tilde{h}_{\ell,1}, \ldots, \tilde{h}_{\ell,q-\ell})'$ is the lower subvector of h_ℓ consisting of unrestricted parameters to be estimated. Thus we have $\theta = (\nu, \mu_1, \delta_1, \sigma_1, \ldots, \mu_q, \delta_q, \sigma_q, \tilde{h}_1', \ldots, \tilde{h}_{q-1}')'$.

Under the assumed specification for Σ_t the measurement density in Equation (37) factorizes as a function in x_t into

$$g_\theta(Y_t|\Sigma_t) = \prod_{\ell=1}^{q} g_\theta(\tilde{y}_{\ell t}|x_{\ell t}), \quad \text{with} \quad g_\theta(\tilde{y}_{\ell t}|x_{\ell t}) \propto \exp\Big\{\frac{\nu}{2}x_{\ell t} - \frac{1}{2}\tilde{y}_{\ell t}\exp(x_{\ell t})\Big\}, \tag{40}$$

where $\tilde{y}_{\ell t} = h_\ell' Y_t^{-1} h_\ell$. It follows that the q state processes $x_{1:T} = (x_{1,1:T}, \ldots, x_{q,1:T})$ are mutually independent under their joint conditional posterior given by

$$p_\theta(x_{1:T}|Y_{1:T}) = \prod_{\ell=1}^{q} p_\theta(x_{\ell,1:T}|Y_{1:T}), \tag{41}$$

$$\text{with} \qquad p_\theta(x_{\ell,1:T}|Y_{1:T}) \propto \left[\prod_{t=2}^{T} g_\theta(\tilde{y}_{\ell t}|x_{\ell t}) f_\theta(x_{\ell t}|x_{\ell t-1})\right] g_\theta(\tilde{y}_{\ell 1}|x_{\ell 1}) f_\theta(x_{\ell 1}), \tag{42}$$

where f_θ represent the Gaussian transitions defined in Equation (39). This independence allows us to parallelize in the PG procedures the conditional SMC step for $p_\theta(x_{1:T}|Y_{1:T})$ by running separately for each $\ell = 1, \ldots, q$ a conditional SMC targeting $p_\theta(x_{\ell,1:T}|Y_{1:T})$. The corresponding parallelized conditional PEIS requires only minor modifications of the PEIS implementation for the univariate SV model in Section 5.2. Essentially, we only need to modify the measurement density g_θ in the (P)EIS target (32) to use for each of the q parallel PEIS runs the associated auxiliary measurement $g_\theta(\tilde{y}_{\ell t}|x_{\ell t})$ as defined in Equation (40), a trivial adjustment altogether.

6.2 Results

The inverted Wishart SSM is applied to $T = 2514$ daily realized covariance matrices observed for $q = 5$ stocks (American Express, Citigroup, General Electric, Home Depot, and IBM). The data spans January 1, 2000 to December, 2009 (for a detailed discussion of this data, see Golosnoy et al., 2012).

We use the PGAS-BPF and PGAS-PEIS for a full posterior MCMC analysis assuming independent conjugate priors for the μ_ℓ's (Gaussian), σ_ℓ^2's (inverse Gaussian) and $\tilde{h}_\ell$'s (Gaussian), and uniform priors for the δ_ℓ's and ν (for details of the prior selection, see Appendix 2). Both PGAS methods are simulated for 15,000 iterations discarding the first 5,000 samples as burn-in. All computations are performed using MATLAB on a 3.1 GHz Intel Core i5 processor. The parallel updating of the state processes $x_{1:T}$ are distributed on 4 cores using the MATLAB function `parfor`. As for the univariate applications, we use for the EIS regressions $R = 15$ trajectories and $L = 4$ iterations.

In Figure 6 we display the update frequencies for the $q = 5$ state processes under the PGAS-BPF with $N = 30$ and $N = 1000$ particles and the PGAS-PEIS with $N = 30$. They reveal that the PGAS-BPF with $N = 30$ suffer from update rates which fall substantially below 50% for many periods leading to $x_{\ell t}^{(j)}$-chains which are stuck for many iterations. Even an increase of the particle number to $N = 1000$ does not fully prevent occasional low update rates. In sharp contrast, the PGAS-PEIS produces with as little as $N = 30$ particles update frequencies which are uniformly close to the maximum ($1 - 1/N \simeq 0.97$) leading to a close to perfect mixing for all the $T \cdot q = 12570$ state variables. In light of those results and the fact that PGAS-BPF with $N = 1000$ takes substantially more CPU time than PGAS-PEIS with $N = 30$ (224.7 versus 132.9 min) we report in Table 5 the posterior parameter estimates only for the PGAS-PEIS ($N = 30$). The reported statistics are sample averages computed from 10 independent replications obtained by running the PGAS-PEIS algorithm under 10 different seeds. All parameter estimates are reasonable. The estimates of the parameters (δ_ℓ,σ_ℓ) reveal that the state processes exhibit substantial variation and strong persistence, which is in full accordance with the results reported by studies of realized (co)variances. The ESS values indicate that even for a challenging specification with as many as 26 parameters and 12,570 state variables the PGAS based on the PEIS is capable to produce numerically accurate and reliable parameter estimates with a fairly moderate computing time.

7. Conclusions

The particle Gibbs (PG) is a flexible and easy to implement tool for conducting Bayesian analyses of state space models. It uses sequential Monte Carlo (SMC) inside the Gibbs procedure in order to update the latent state trajectories. However, in high-dimensional applications when there is path degeneracy in the underlying SMC sampler the baseline PG suffers from severe mixing problems. Refinements designed to improve the mixing of the baseline PG introduce an ancestor sampling step to the underlying SMC (PGAS) or an additional Metropolis-Hastings move for the update of the state trajectories (PGMH). However, such refinements when implemented using a standard locally designed SMC procedure such as the bootstrap particle filter of Gordon et al. (1993) can still be prone to mixing problems, particularly, in applications involving narrowly distributed measurement variables and given the presence of outliers.

Here, we have proposed to combine the PG and its refinements with Particle Efficient Importance Sampling (PEIS) to overcome the mixing problem of the PG. The PEIS is an SMC algorithm based on a recursive sequence of simple auxiliary regressions designed to construct highly efficient SMC importance sampling densities and resampling weights, which are globally adapted to the targeted posterior density of the states. We have shown that the PG when combined with PEIS leads to significant improvements of the mixing w.r.t. the state trajectories relative to PG procedures based on standard locally designed SMC algorithms. By such improvements of the mixing, PG implementations based on PEIS allow for numerically accurate and reliable Bayesian parameter estimates not only in univariate state space models but also in multivariate high-dimensional specifications as illustrated by the applications to a stochastic volatility model for asset returns, a constant elasticity of variance model for interest rates and an inverted Wishart model for the realized covariance matrix of asset returns.

Acknowledgements

We thank participants of the 2015 Rhenisch Multivariate Time Series Econometrics (RMSE) Meeting (University of Cologne) and of the CMStatistics 2015 (ERCIM 2015) conference, London. We thank Yacine Aït-Sahalia for sharing the Eurodollar data used in Aït Sahalia (1996). We are grateful to the Regional Computing Center at the University of Cologne for providing parts of the computational resources required. R. Liesenfeld acknowledges support by the Deutsche Forschungsgemeinschaft (grant LI 901/3-1).

Appendix 1: Proof of Lemma 1

In order to obtain the relationship between the predictive density $p_\theta(y_{t+1:T}|x_t)$ and the EIS integrating factor $\chi_{t+1}(x_{1:t};c_t)$ defined in Equation (12), we first write the predictive densities for the SSM given in Equation (1) as the following backward-recursive sequence of integrals:

$$p_\theta(y_T|x_{T-1}) = \int g_\theta(y_T|x_T) f_\theta(x_T|x_{T-1}) dx_T, \tag{43}$$

$$p_\theta(y_{t:T}|x_{t-1}) = \int p_\theta(y_{t+1:T}|x_t) g_\theta(y_t|x_t) f_\theta(x_t|x_{t-1}) dx_t, \qquad t = T-1, ..., 2, \tag{44}$$

$$p_\theta(y_{1:T}) = \int p_\theta(y_{2:T}|x_1) g_\theta(y_1|x_1) f_\theta(x_1) dx_1. \tag{45}$$

This sequence shows that if the period-T EIS-kernel $k_T(x_{1:T};\hat{c}_T)$ as a function in $x_{T-1:T}$ is close to be proportional to the integrand $g_\theta(y_T|x_T)f_\theta(x_T|x_{T-1})$ in Equation (43), then (i) its integrating factor $\chi_T(x_{1:T-1};\hat{c}_T)$ is close to be proportional to the density $p_\theta(y_T|x_{T-1})$ as a function in x_{T-1}, and (ii) we obtain the following close approximation to the period $T-1$ integrand as given by Equation (44)

$$p_\theta(y_T|x_{T-1}) g_\theta(y_{T-1}|x_{T-1}) f_\theta(x_{T-1}|x_{T-2}) \simeq \tag{46}$$

$$\text{constant} \cdot \chi_T(x_{1:T-1}, \hat{c}_T) g_\theta(y_{T-1}|x_{T-1}) f_\theta(x_{T-1}|x_{T-2}),$$

where the r.h.s is approximated by the period-$(T-1)$ EIS density kernel $k_{T-1}(x_{1:T-1};\hat{c}_{T-1})$. The proof of Equation (18) follows by recursion and the fact that $\{k_t(x_{1:t};\hat{c}_t)\}$ are designed to approximate back-recursively $\{g_\theta(y_t|x_t)f_\theta(x_t|x_{t-1})\chi_{t+1}(x_{1:t},\hat{c}_{t+1})\}$ as close as possible (see Equation 14).

From the interpretation of χ_{t+1} given in Equation (18) it immediately follows that

$$q_t(x_t|x_{1:t-1};\hat{c}_t) = \frac{k_t(x_{1:t};\hat{c}_t)}{\chi_t(x_{1:t-1},\hat{c}_t)} \simeq \frac{g_\theta(y_t|x_t) f_\theta(x_t|x_{t-1}) p_\theta(y_{t+1:T}|x_t)}{p_\theta(y_{t:T}|x_{t-1})} = p_\theta(x_t|x_{t-1}, y_{t:T}), \tag{47}$$

as stated in Equation (19).

Appendix 2: Prior assumptions

SV and CEV model. For the parameters of the SV model in Equations (28) and (29) we use the following priors: For $\ln\beta$ we assume a flat prior, and for $(\delta+1)/2$ a Beta prior with a prior mean for δ of

0.86 and a prior variance of 0.012. For ν^2 an inverted chi-squared prior with $\nu^2 \sim p_0 s_0/\chi^2_{(p_0)}$ and $p_0 = 10$ and $s_0 = 0.01$ is used. The conditional posteriors for β and ν can be simulated directly. To sample from the conditional posterior of δ we use an independent MH sampler (for details, see Kim et al., 1998).

The prior assumptions on the parameters of the CEV model in Equation (30) and (31) are the following: for α and β we assume a Gaussian prior with $\alpha \sim N(0, 1000)$ and $\beta \sim N(0, 1000)$ and for γ a uniform pior on the interval $[0, 4]$. An uninformative inverted chi-squared prior is used for σ_x^2 and σ_y^2 with prior densities given by $p(\sigma_x^2) \propto 1/\sigma_x^2$ and $p(\sigma_y^2) \propto 1/\sigma_y^2$. All conditional posteriors in the CEV model are of known form, except for that of γ, which we sample using Griddy Gibbs.

Inverted Wishart model. For the inverted Wishart model in Equations (37)-(39) we use for μ_ℓ and $\tilde{h}_{\ell,m}$ ($\ell = 1, \ldots, q$,$m = 1, \ldots, q - \ell$) independent Gaussian priors given by $\mu_\ell \sim N(0, 25)$ and $\tilde{h}_{\ell,m} \sim N(0, 100)$, for σ_ℓ^2 inverted chi-square priors given by $\sigma_\ell^2 \sim p_0 s_0/\chi^2_{(p_0)}$ with $p_0 = 4$ and $s_0 = 0.25$, for δ_ℓ uniform priors on $[-1, 1]$, and for ν a uniform prior on the discrete grid $[q + 2, q + 2 + 0.01, q + 2 + 0.02, \ldots, 200]$. All conditional posteriors are of known form and are simulated directly except those for the δ_ℓ's which we update using independent MH.

References

Aït-Sahalia, Y., 1996. Testing continuous-time models of the spot interest rate. Review of Financial Studies 9, 385-426.

Aït-Sahalia, Y., 1999. Transition densities for interest rate and other nonlinear diffusions. Journal of Finance 54, 1361-1395.

Anderson, T.W., 1984. An Introduction to Multivariate Statistical Analysis. John Wiley & Sons, New York.

Andrieu, C., Doucet, A., and Holenstein, R., 2010. Particle Markov Chain Monte Carlo methods. Journal of the Royal Statistical Society 72, Series B, 269-342.

Barndorff-Nielsen, O.E, Shephard, N., 2004. Econometric analysis of realized covariation: high frequency based covariance, regression, and correlation in financial economics. Econometrica 72, 885-925.

Cappé, O., Godsill, S.J., and Moulines, E., 2007. An overview of exsting methods and recent advances in sequential Monte Carlo. Proceedings of the IEEE 95, 899-924.

Carter, C.K., Mendes E.F., and Kohn, R., 2014. An extended space approach for particle Markov chain Monte Carlo methods. Working paper, eprint arXiv:1406.5795.

Chan, K.C., Karolyi, G.A., Longstaff, F.A., and Sanders, A.B., 1992. An empirical comparison of alternative models of the short-term interest rate. Journal of Finance 47, 1209-1227.

Chopin, N., and Singh, S.S., 2013. On the particle Gibbs sampler. Working paper, eprint arXiv:1304.1887.

DeJong, D.N., Liesenfeld, R., Moura, G.V., Richard, J.-F., and Dharmarajan, H., 2013. Efficient likelihood evaluation of state-space representations. The Review of Economic Sudies 80, 538-567

Doucet, A., and Johansen, A.M., 2009. A tutorial on particle filtering and smoothing: Fifteen years later. In: Crisan, D., Rozovskii, B. (eds), The Oxford Handbook of Nonlinear Filtering. Oxford University Press, 656-704.

Fernandez-Villaverde, J., and Rubio-Ramirez, J.F., 2005. Estimating dynamic equilibrium economies: Linear versus nonlinear likelihood. Journal of Applied Econometrics 20, 891-910.

Flury, T., and Shephard, N., 2011. Bayesian inference based only on simulated likelihood: Particle filter analysis of dynamic economic models. Econometric Theory 27, 933-956.

Geyer, C.J., 1992. Practical Markov Chain Monte Carlo. Statistical Science 7, 473-483.

Ghysels, E., Harvey, A., and Renault, E., 1996. Stochastic Volatility. In: Maddala, G., Rao, C.R. (eds), Handbook of Statistics, Vol 14. Elsevier Sciences, 119-191.

Golosnoy, V., Gribisch, B., Liesenfeld, R. 2012. The conditional autoregressive Wishart model for multivariate stock market volatility. Journal of Econometrics 167, 211-223.

Gordon, N.J., Salmond, D.J., and Smith, A.F.M., 1993. A novel approach to non-linear and non-Gaussian Bayesian state estimation. IEEE Proceedings-F 140, 107-113.

Holenstein, R., 2009. Particle Markov Chain Monte Carlo. PhD-Thesis, University of British Colombia.

Jin, X., Maheu, J.M., 2016. Bayesian semiparametric modeling of realized covariance matrices. Journal of Econometrics 192, 19-39.

Kim, S., Shephard, N., and Chib, S., 1998. Stochastic volatility: Likelihood inference and comparison with ARCH models. Review of Economic Studies 65, 361-393.

Kleppe, T.S., 2016. Adaptive step size selection for Hessian-based manifold Langevin samplers. Scandinavian Journal of Statistics 43, 788-805.

Kleppe, T.S., and Liesenfeld, R., 2014. Efficient importance sampling in mixture frameworks. Computational Statistics and Data Analysis 76, 449-463.

Kleppe, T.S., and Skaug, H.J., 2015. Bandwidth selection in pre-smoothed particle filters. Statistics and Computing, in press (DOI 10.1007/s11222-015-9591-4).

Lindsten, F., Doucet, A., 2016. Pseudo-Marginal Hamiltonian Monte Carlo. Working paper, eprint arXiv:1607.02516,

Lindsten, F., Jordan, M.I., and Schön, T.B., 2014. Particle Gibbs with ancestor sampling. Journal of Machine Learning Research 15, 2145-2184.

Lindsten, F., and Schön, T.B., 2012. On the use of backward simulation in particle Markov chain Monte Carlo methods. Working paper, Linköping University, Sweden.

Liu, J.S., 1994. The collapsed Gibbs sampler in Bayesian computations with a applications to a gene regulation problem. Journal of the American Statistical Association 89, 958-966.

Pitt, M.K., Hall, J., and Kohn, R., 2015. Bayesian inference for latent factor GARCH models. Working paper, eprint arXiv:1507.01179.

Pitt, M.K., Silva, d.S.R., Giordani, P., Kohn, R., 2012. On some properties of Markov chain Monte Carlo simulation methods based on the particle filter. Journal of Econometrics 171, 134-151.

Pitt, M.K., Shephard, N., 1999. Filtering via simulation: Auxiliary particle filters. Journal of the American Statistical Association 94, 590-599.

Richard, J.-F., Zhang, W., 2007. Efficient high-dimensional importance sampling. Journal of Econometrics 141, 1385-1411.

Ristic, B., Arulampalam, S., Gordon, N., 2004. Beyond the Kalman Filter: Particle Filters for Tracking Applications. Artech House, Boston.

Scharth, M., and Kohn, R., 2016. Particle Efficient Importance Sampling. Journal of Econometrics 190, 133-147.

Tsay, R.S., 2010. Analysis of Financial Time Series. John Wiley & Sons, Hoboken, New Jersey.

Whiteley, N., 2010. Discussion on: Particle Markov Chain Monte Carlo methods. Journal of the Royal Statistical Society 72, Series B, 306-307.

Whiteley, N., Andrieu, C., Doucet, A., 2010. Efficient Bayesian inference for switching state space models using discrete particle Markov chain Monte Carlo methods. Bristol Statistics Research Report 10:04, University of Bristol.

Zhang, Y., and Sutton, C., 2011. Quasi-Newton Methods for Markov chain Monte Carlo. In: Shawe-Taylor, J., Zemel, R.S., Bartlett, P.L., Periera, F., Weinberger, K.Q. (eds), Advances in Neural Information Processing Systems (NIPS), 2393-2401.

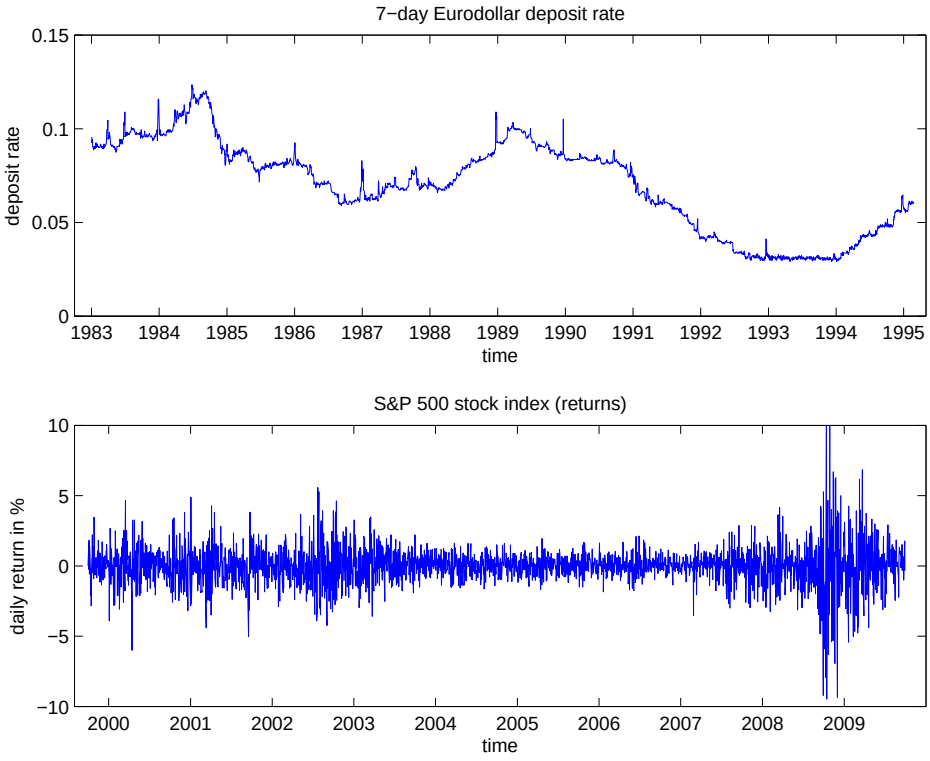

Figure 1. Top panel: The daily short-term Eurodollar interest rates from 1983 to 1995; Bottom panel: The daily returns on the S&P 500 stock index from 1999 to 2009.

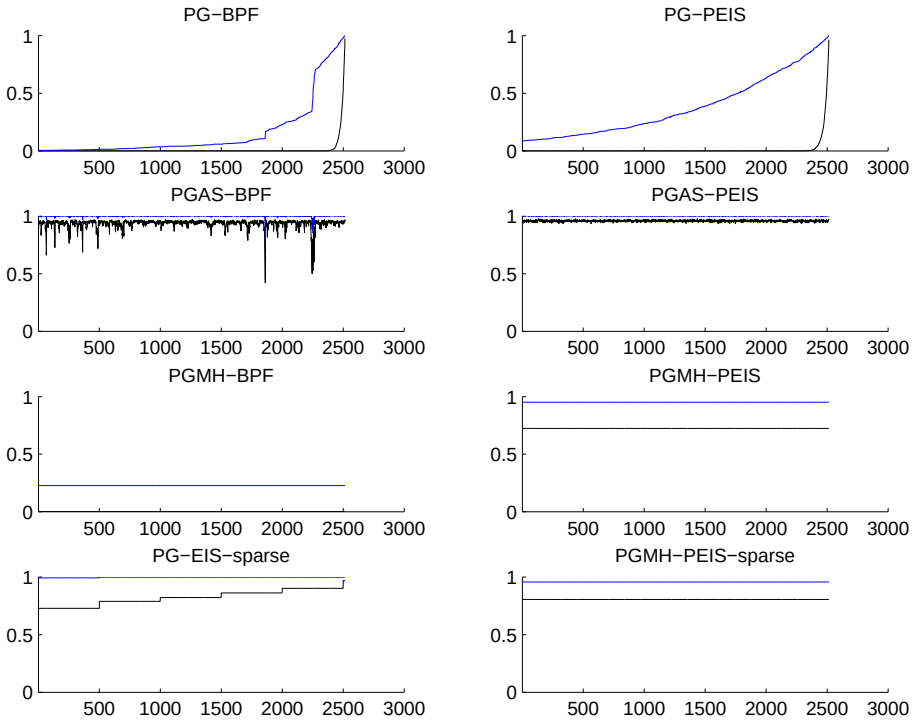

Figure 2. PG update rates for x_t versus $t = 1, ..., T$ for the SV model, using $N = 30$ particle (black line) and $N = 1000$ (blue line).

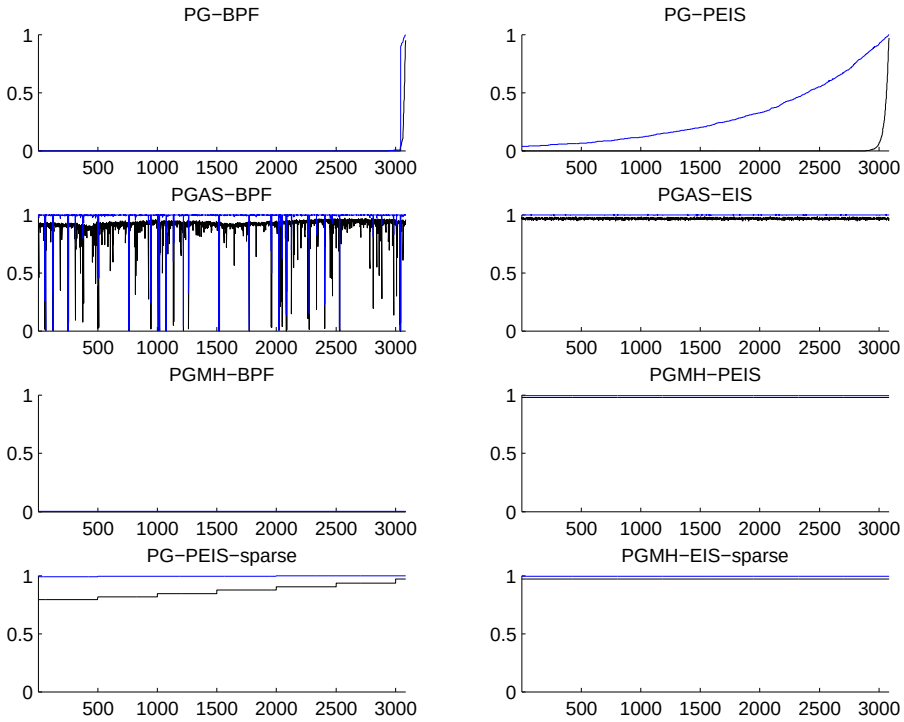

Figure 3. PG update rates for x_t versus $t = 1, ..., T$ for the CEV model, using $N = 30$ particle (black line) and $N = 1000$ (blue line).

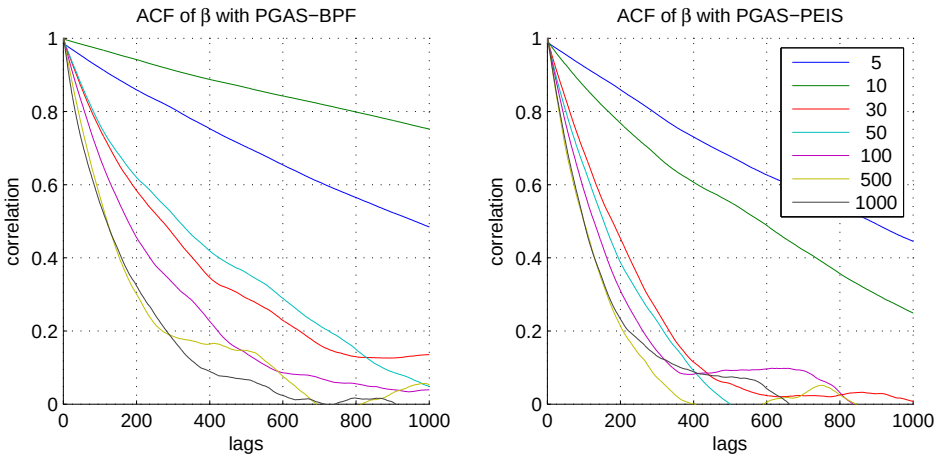

Figure 4. ACFs of the sampled SV parameter β for PGAS-BPF (left) and PGAS-PEIS (right) under different numbers of SMC particles, $N \in \{5, 10, 30, 50, 100, 500, 1000\}$.

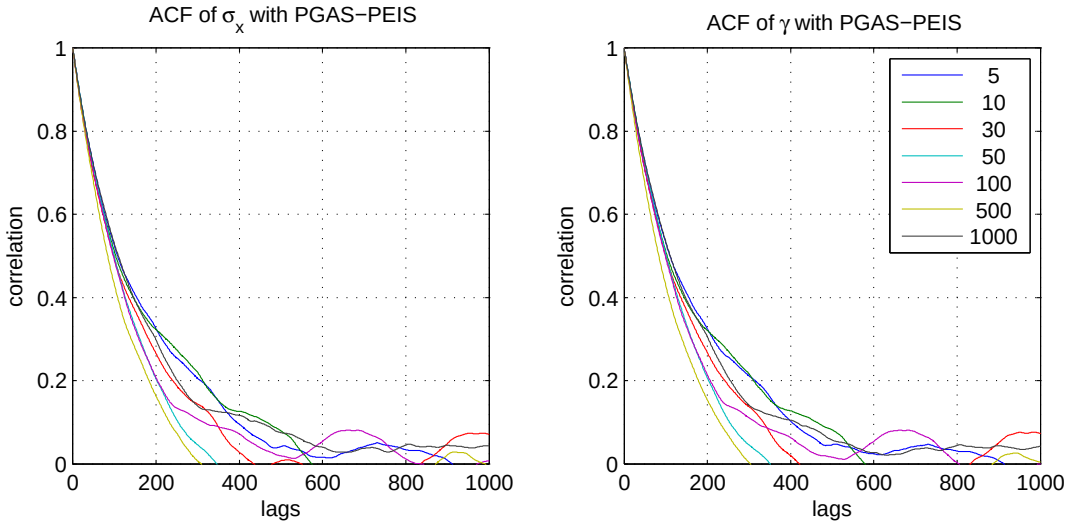

Figure 5. ACFs of the sampled CEV parameters σ_x (left) and γ (right) for the PGAS-PEIS under different numbers of SMC particles, $N \in \{5, 10, 30, 50, 100, 500, 1000\}$.

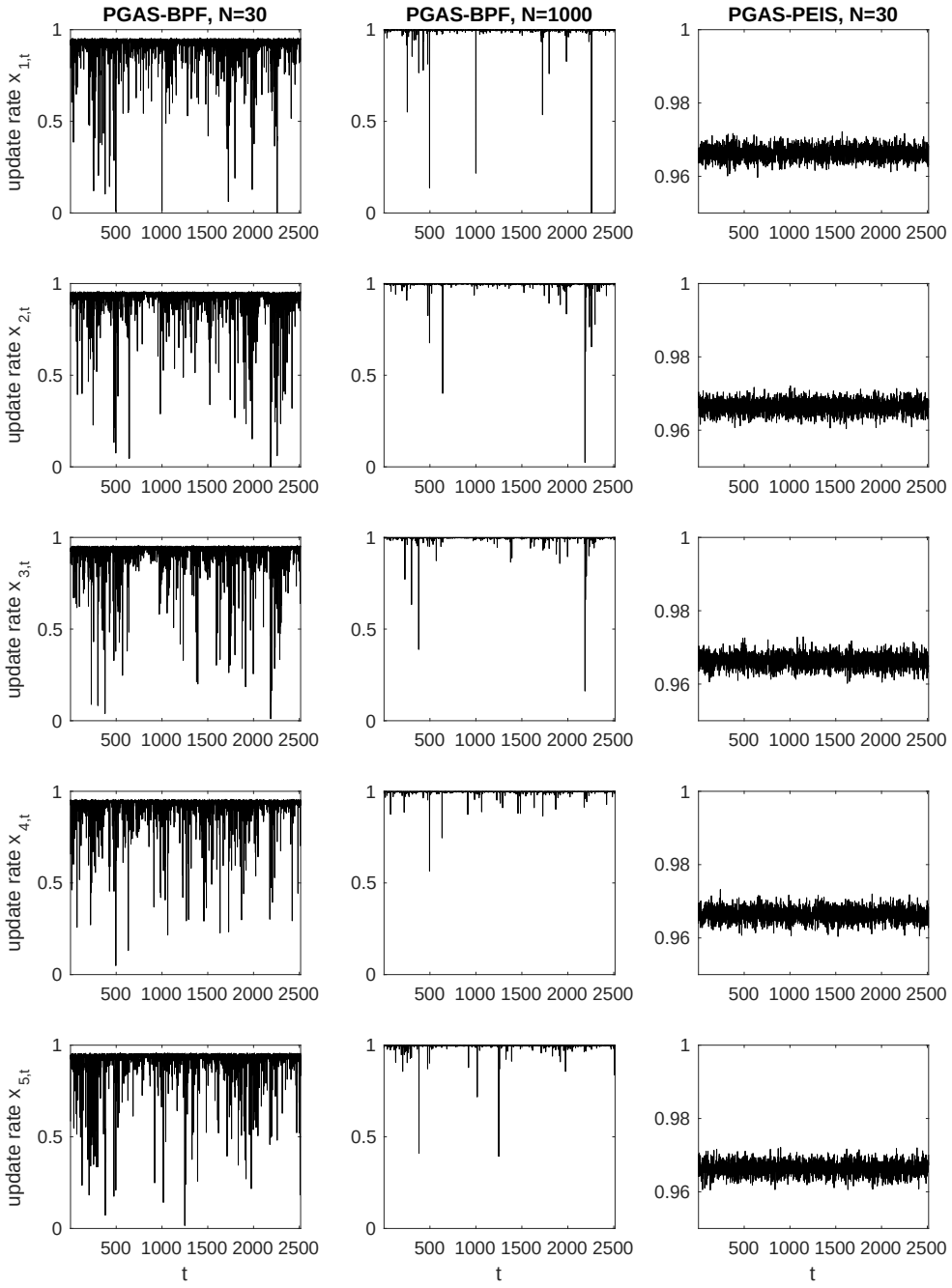

Figure 6. PGAS update rates for $x_t = (x_{1t}, \ldots, x_{5t})$ versus $t = 1, ..., T$ for the inverted Wishart model under the BPF with $N = 30$ (left panel), BPF with $N = 1000$ (middle panel), PEIS with $N = 30$ (right panel).

Table 1. Effective Sample Size for PG Samples from the Posterior of the States in the SV Model for Fixed Parameters

	Number of particles	CPU time in sec	Minimum ESS	Median ESS	Maximum ESS	Minimum ESS per hour CPU time
PG-BPF	30	283	1	1	621	13
PG-BPF	1000	942	3	30	1000	12
PG-PEIS	30	1646	1	1	566	2
PG-PEIS	1000	2397	21	173	999	31
PG-PEIS-sparse	30	1552	332	671	969	771
PG-PEIS-sparse	1000	2249	569	948	1000	912
PGAS-BPF	30	653	45	415	689	254
PGAS-BPF	1000	1499	297	934	1000	716
PGAS-PEIS	30	2042	240	475	707	423
PGAS-PEIS	1000	3038	573	949	1000	686
PGMH-BPF	30	881	1	1	1	4
PGMH-BPF	1000	2454	34	113	210	51
PGMH-PEIS	30	2313	284	538	756	442
PGMH-PEIS	1000	3798	532	876	1000	505
PGMH-PEIS-sparse	30	1906	355	662	860	674
PGMH-PEIS-sparse	1000	3345	552	894	1000	563

NOTE: Results from the PG algorithms are based on 1,100 PG iterations (discarding the first 100 draws). All reported statistics are sample averages computed from 10 independent replications of the PG algorithms under 10 different seeds.

Table 2. Effective Sample Size for PG Samples from the Posterior of the States in the CEV Model for Fixed Parameters

	Number of particles	CPU time in sec	Minimum ESS	Median ESS	Maximum ESS	Minimum ESS per hour CPU time
PG-BPF	30	159	1	1	926	23
PG-BPF	1000	1241	1	1	1000	3
PG-PEIS	30	1228	1	1	916	3
PG-PEIS	1000	3074	10	125	1000	11
PG-PEIS-sparse	30	1148	368	739	1000	1154
PG-PEIS-sparse	1000	2853	555	962	1000	701
PGAS-BPF	30	302	1	871	1000	12
PGAS-BPF	1000	2166	2	963	1000	3
PGAS-PEIS	30	1325	522	902	1000	1421
PGAS-PEIS	1000	3916	545	967	1000	501
PGMH-BPF	30	436	36	36	36	278
PGMH-BPF	1000	2723	9	9	11	12
PGMH-PEIS	30	1628	522	924	1000	1156
PGMH-PEIS	1000	5271	565	961	1000	386
PGMH-PEIS-sparse	30	1404	512	929	1000	1314
PGMH-PEIS-sparse	1000	4727	549	963	1000	418

NOTE: Results from the PG algorithms are based on 1,100 PG iterations (discarding the first 100 draws). All reported statistics are sample averages computed from 10 independent replications of the PG algorithms under 10 different seeds.

Table 3. PG Posterior Analysis of the SV Model

		PG-PEIS-sparse	PGAS-BPF	PGAS-PEIS	PGMH-PEIS	PGMH-PEIS-sparse	Ideal Gibbs
	CPU time (hours)	14:30	5:49	18:45	21:26	17:15	
β	post. mean	1.0617	1.0645	1.0754	1.0580	1.0727	1.0708
	post. std.	0.1855	0.1943	0.1892	0.2214	0.1978	0.2003
	ESS	96	41	77	72	96	112
	ESS/hour CPU time	7	7	4	3	6	
δ	post. mean	0.9924	0.9924	0.9924	0.9926	0.9924	0.9924
	post. std.	0.0027	0.0027	0.0027	0.0028	0.0027	0.0028
	ESS	653	467	582	474	538	694
	ESS/hour CPU time	45	80	31	22	31	
ν	post. mean	0.1205	0.1204	0.1201	0.1203	0.1202	0.1206
	post. std.	0.0125	0.0125	0.0125	0.0123	0.0125	0.0128
	ESS	265	345	355	226	251	356
	ESS/hour CPU time	18	59	19	11	15	
x_1	post. mean	0.4246	0.4250	0.4032	0.4531	0.4101	0.4141
	post. std.	0.4997	0.5160	0.5092	0.5514	0.5109	0.5210
	ESS	263	108	204	198	251	261
	ESS/hour CPU time	18	18	11	9	15	
$x_{T/2}$	post. mean	-0.8114	-0.8136	-0.8347	-0.7794	-0.8281	-0.8229
	post. std.	0.4443	0.4600	0.4520	0.5054	0.4540	0.4678
	ESS	172	72	135	125	171	184
	ESS/hour CPU time	12	12	7	6	10	
x_T	post. mean	-0.2229	-0.2253	-0.2432	-0.1903	-0.2377	-0.2335
	post. std.	0.5091	0.5229	0.5154	0.5618	0.5208	0.5271
	ESS	273	113	211	202	252	277
	ESS/hour CPU time	19	19	11	9	15	

NOTE: Results from the PG algorithms for the stochastic volatility model based on 50,000 PG iterations (discarding the first 10,000 draws) and $N = 30$ SMC particles. All reported statistics are sample averages computed from 10 independent replications of the PG algorithms under 10 different seeds. The ML estimates for the parameters are $(\beta, \delta, \nu) = (1.065, 0.992, 0.122)$.

Table 4. PG Posterior Analysis of the CEV Model

		PG-PEIS-sparse	PGAS-BPF	PGAS-PEIS	PGMH-PEIS	PGMH-PEIS-sparse	Ideal Gibbs
	CPU time (hours)	20:56	7:45	20:05	23:44	17:47	
α	post. mean	0.0099	0.0067	0.0099	0.0098	0.0098	0.0099
	post. std.	0.0090	0.0068	0.0090	0.0090	0.0090	0.0090
	ESS	35188	–	34896	35144	35544	34396
	ESS/hour CPU time	1682	–	1738	1481	1998	
β	post. mean	0.1685	0.1297	0.1682	0.1675	0.1682	0.1683
	post. std.	0.1727	0.1312	0.1726	0.1727	0.1728	0.1727
	ESS	37493	–	37689	37083	37407	37252
	ESS/hour CPU time	1792	–	1878	1563	2103	
σ_x	post. mean	0.4058	0.3046	0.4074	0.4080	0.4071	0.4074
	post. std.	0.0602	0.0570	0.0594	0.0634	0.0609	0.0616
	ESS	141	–	149	122	137	137
	ESS/hour CPU time	7	–	7	5	8	
γ	post. mean	1.1813	1.1744	1.1830	1.1831	1.1826	1.1828
	post. std.	0.0589	0.0711	0.0576	0.0609	0.0592	0.0593
	ESS	139	–	147	122	134	136
	ESS/hour CPU time	7	–	7	5	8	
σ_y	post. mean	0.0005	0.0009	0.0005	0.0005	0.0005	0.0005
	post. std.	2.3e-5	1.9e-5	2.2e-5	2.3e-5	2.3e-5	2.2e-5
	ESS	675	–	770	629	587	723
	ESS/hour CPU time	32	–	38	27	33	
x_1	post. mean	0.0954	0.0949	0.0954	0.0954	0.0954	0.0954
	post. std.	0.0005	0.0008	0.0005	0.0005	0.0005	0.0005
	ESS	36784	–	36900	37346	25507	39114
	ESS/hour CPU time	1759	–	1837	1574	1435	
$x_{T/2}$	post. mean	0.0925	0.0924	0.0925	0.0925	0.0925	0.0925
	post. std.	0.0005	0.0007	0.0005	0.0005	0.0005	0.0005
	ESS	37733	–	36712	37810	30781	39671
	ESS/hour CPU time	1804	–	1828	1594	1731	
x_T	post. mean	0.0608	0.0607	0.0608	0.0608	0.0608	0.0608
	post. std.	0.0005	0.0007	0.0005	0.0005	0.0005	0.0005
	ESS	37503	–	36689	37834	36953	39638
	ESS/hour CPU time	1792	–	1827	1595	2078	

NOTE: Results from the PG algorithms for the CEV interest rate model based on 50,000 PG iterations (discarding the first 10,000 draws) and $N = 30$ SMC particles. All reported statistics are sample averages computed from 10 independent replications of the PG algorithms under 10 different seeds. The ML estimates for the parameters are $(\alpha, \beta, \sigma_x, \gamma, \sigma_y)$ = (0.0097, 0.1656, 0.4250, 1.201, 0.0005).

Table 5. PGAS-PEIS Posterior Analysis of the Inverted-Wishart Model

	μ_1	μ_2	μ_3	μ_4	μ_5	δ_1	δ_2	δ_3	δ_4	δ_5
post. mean	4.15	4.12	3.72	4.11	3.53	0.97	0.98	0.96	0.94	0.96
post. std.	0.20	0.26	0.15	0.10	0.13	0.005	0.004	0.006	0.008	0.006
ESS	9815	9731	9369	9326	9571	4101	4622	4162	2904	3159
	σ_1	σ_2	σ_3	σ_4	σ_5	ν				
post. mean	0.31	0.26	0.29	0.28	0.25	33.6				
post. std.	0.009	0.008	0.009	0.009	0.009	0.28				
ESS	1044	1032	1053	944	809	275				
	$\tilde{h}_{1,1}$	$\tilde{h}_{1,2}$	$\tilde{h}_{1,3}$	$\tilde{h}_{1,4}$	$\tilde{h}_{2,1}$	$\tilde{h}_{2,2}$	$\tilde{h}_{2,3}$	$\tilde{h}_{3,1}$	$\tilde{h}_{3,2}$	$\tilde{h}_{4,1}$
post. mean	0.39	0.29	0.29	0.23	0.20	0.17	0.12	0.22	0.18	0.11
post. std.	0.003	0.003	0.003	0.002	0.003	0.003	0.002	0.004	0.003	0.002
ESS	8260	8566	8860	8398	8530	7828	7274	9173	9046	9413

NOTE: Results based on 15,000 PGAS-PEIS iterations (discarding the first 5,000 draws) and $N = 30$ SMC particles. All reported statistics are sample averages computed from 10 independent replications of the PGAS-PEIS algorithms under 10 different seeds.